On nonlinear convection in mushy layers. Part 2. Mixed oscillatory and stationary modes of convection

By D. N. RIAHI

Department of theoretical and Applied Mechanics, 216 Talbot Laboratory, 104 South Wright Street, University of Illinois at Urbana-Champaign, Urbana, IL 61801, USA

This paper presents part 2 of a study of nonlinear convection in horizontal mushy layers during the solidification of binary alloys. Part 1 dealt with only the oscillatory modes of convection (Riahi, *J. Fluid Mech.* vol. 467, 2002, pp. 331–359). In the present paper we consider the particular range of parameters where the critical values of the scaled Rayleigh number R for the onset of oscillatory and stationary convection are close to each other, and we develop and analyse a nonlinear theory in such a parameter regime which takes into account those mixed stationary and oscillatory modes of convection with common wavenumber vectors. Under a near-eutectic approximation and in the limit of large far-field temperature, we first determine a number of weakly nonlinear solutions, and then the stability of these solutions is investigated. The most interesting result is the preference for a mixed solution composed of standing and stationary hexagonal modes over a relatively wide range of the parameter values and for R just above its lowest subcritical value where convection is possible. Such a preferred solution has properties mostly in agreement with the experimental results due to Tait *et al.* (*Nature*, vol. 359, 1992, pp. 406–408) in the sense that the flow is downward at the cell centres, upward at the cell boundaries and there is some tendency for channel formation at the cell nodes.

1. Introduction

In part 1 (Riahi 2002) the problem of nonlinear convection in horizontal mushy layers during the solidification of binary alloys was studied. The oscillatory modes of convection were analysed in a particular range of the parameter values where the critical value $R_c^{(o)}$ of the scaled Rayleigh number R for the onset of oscillatory convection is distinctly lower than the critical value $R_c^{(s)}$ of R for the onset of stationary convection. The results indicated a preference for supercritical simple travelling rolls over most of the range of parameter values studied, while supercritical standing rolls were preferred only over a rather small range of the parameter values. That detailed nonlinear study of the oscillatory modes of convection in mushy layers complemented previous nonlinear studies of stationary convection in mushy layers (Amberg & Homsy1993; Anderson & Worster 1995).

The motivation and justification for the present investigation was due to the realization that, under the already established relevant scaling (Anderson & Worster 1995, 1996), the linear system of the problem in a particular range of the parameter values exhibits both oscillatory and stationary modes of convection at very close values of $R_c^{(o)}$ and $R_c^{(s)}$. This particular range of the parameter values was found to

cover that of the available experimental results (Tait, Jahrling & Jaupart 1992). Hence, to determine the analytical results, which can be applicable to such a range of the parameter values and, in particular, can be compared with the available experimental results (Tait *et al.* 1992) with some confidence, the present nonlinear theory for the mixed modes of oscillatory and stationary convection was developed and analysed.

The present theory was first motivated by the work of Busse & Riahi (1988) for the mixed-mode patterns of bifurcations from spherically symmetric basic states. These authors determined a number of new patterns which are likely to occur in bifurcations from spherically symmetric basic states when two neighbouring degrees l and l^* of spherical harmonics yield nearly the same lowest value of the control parameter R. Their preferred solutions were based on an assumption of the type adopted previously by Busse (1975) that the solution that exists at the lowest value of the control parameter R is the physically preferred solution. This assumption follows from the stability results (Busse 1967; Riahi 1983). In the present paper we follow Busse (1975) and Busse & Riahi (1988) and, in addition, carry out a stability analysis of the finite-amplitude solutions to determine the preferred solutions.

The following two sections (2, 3) deal with the governing system and the finite-amplitude and stability analyses. The results of the mixed solutions and their stability are presented and discussed in §4, which is followed by conclusion and remarks in §5.

2. Governing system

We consider a binary alloy melt that is cooled from below and is solidified at a constant speed V_0. Following Amberg & Homsy (1993) and Anderson & Worster (1995), we consider a horizontal mushy layer of thickness d adjacent to and above the solidification front to be physically isolated from the overlying liquid and underlying solid zones. The overlying liquid is assumed to have a composition $C_0 > C_e$ and temperature $T_\infty > T_L(C_0)$ far above the mushy layer, where C_e is the eutectic composition, $T_L(\tilde{C})$ is the liquidus temperature of the alloy and $\tilde{C}$ is the composition. It is then assumed that the horizontal mushy layer is bounded from above and below by rigid and isothermal boundaries. We consider the solidification system in a moving frame of reference $o\tilde{x}\tilde{y}\tilde{z}$, whose origin lies on the solidification front and translating at the speed V_0 with the solidification front in the positive $\tilde{z}$-direction. The reader is referred to part 1 for the motivation and justification in using the Amberg & Homsy (1993) type of model for the present study.

The equations for Darcy-momentum, continuity, heat and solute for the flow in the mushy layer in the moving frame described above are non-dimensionalized by using V_0, k/V_0, k/V_0^2, $\beta\Delta C\rho g k/V_0$, ΔC and ΔT as scales for velocity, length, time, pressure, solute and temperature, respectively. Here k is the thermal diffusivity, ρ is a reference (constant) density, $\beta = \beta^* - \Gamma\alpha^*$, where α^* and β^* are the expansion coefficients for the heat and solute, respectively, and Γ is the slope of the liquidus, which is assumed to be a constant, $\Delta C = C_0 - C_e$, $\Delta T = T_L(C_0) - T_e$ and T_e is the eutectic temperature. The non-dimensional form of the equations for Darcy-momentum, continuity, temperature and solute concentration in the mushy layer are then

$$\mathrm{K}(\tilde{\phi})\tilde{\boldsymbol{u}} = -\nabla\tilde{P} - \tilde{R}\tilde{\theta}z, \tag{1a}$$

$$\nabla\cdot\tilde{\boldsymbol{u}} = 0, \tag{1b}$$

$$\left(\frac{\partial}{\partial\tilde{t}} - \frac{\partial}{\partial\tilde{z}}\right)(\tilde{\theta} - S_t\tilde{\phi}) + \tilde{\boldsymbol{u}}\cdot\nabla\tilde{\theta} = \nabla^2\tilde{\theta}, \tag{1c}$$

$$\left(\frac{\partial}{\partial \tilde{t}} - \frac{\partial}{\partial \tilde{z}}\right)[(1-\tilde{\phi})\tilde{\theta} + C_r\tilde{\phi}] + \tilde{\boldsymbol{u}}\cdot\nabla\tilde{\theta} = 0, \tag{1d}$$

where $\tilde{\boldsymbol{u}} = \tilde{u}\boldsymbol{x} + \tilde{v}\boldsymbol{y} + \tilde{w}\boldsymbol{z}$ is the volume flux per unit area, $\tilde{u}$ and $\tilde{v}$ are the horizontal components of $\tilde{\boldsymbol{u}}$ in the $\tilde{x}$- and $\tilde{y}$-directions, respectively, $\boldsymbol{x}$ and $\boldsymbol{y}$ are unit vectors in the positive $\tilde{x}$- and $\tilde{y}$-directions, $\tilde{w}$ is the vertical component of $\tilde{\boldsymbol{u}}$ in the $\tilde{z}$-direction, $\boldsymbol{z}$ is a unit vector in the positive $\tilde{z}$-direction, $\tilde{P}$ is the modified pressure, $\tilde{\theta}$ is the non-dimensional form of either composition or temperature as shown in part 1, $\tilde{t}$ is the time variable, $\tilde{\phi}$ is the local solid fraction, $\tilde{R} = \beta\Delta Cg\Pi(0)/(V_0\nu)$ is the Rayleigh number, $\Pi(0)$ is reference value at $\tilde{\phi}=0$ of the permeability $\Pi(\tilde{\phi})$ of the porous medium, ν is the kinematic viscosity, g is acceleration due to gravity, $K(\tilde{\phi}) \equiv \Pi(0)/\Pi(\tilde{\phi})$, $S_t = L/(C_L\Delta T)$ is the Stefan number, C_L is the specific heat per unit volume, L is the latent heat of solidification per unit volume, $C_r = (C_s - C_0)/\Delta C$ is a concentration ratio, and C_s is the composition of the solid phase forming the dendrites. Equation (1d) is based on the limit of sufficiently large value of the Lewis number k/k_s, where k_s is the solute diffusivity. The above equations are subject to the following boundary conditions:

$$\tilde{\theta} + 1 = \tilde{w} = 0 \quad \text{at} \quad \tilde{z} = 0, \tag{1e}$$

$$\tilde{\theta} = \tilde{w} = \tilde{\phi} = 0 \quad \text{at} \quad \tilde{z} = \delta, \tag{1f}$$

where $\delta = dV_0/k$ is a growth Peclet number representing the dimensionless depth of the layer.

Next, we consider the following rescaling in the limit of sufficiently small δ:

$$C_r = \frac{C}{\delta}, \quad S_t = \frac{S}{\delta}, \quad \varepsilon \ll \delta \ll 1, \tag{2a}$$

$$(\tilde{x}, \tilde{y}, \tilde{z}) = \delta(x, y, z), \quad \tilde{t} = \delta^2 t, \quad R^2 = \delta\tilde{R}, \tag{2b}$$

$$(\tilde{\theta}, \tilde{\phi}, \tilde{\boldsymbol{u}}, \tilde{P}) = (\theta_B, \phi_B, 0, P_B) + \varepsilon[\theta(x, y, z, t), \phi(x, y, z, t),$$
$$(R/\delta)\boldsymbol{u}(x, y, z, t), RP(x, y, z, t)], \tag{2c}$$

where C and S are order-one quantities as $\delta \to 0$, ε is small perturbation amplitude, and the quantities with subscript 'B' are the basic flow variables for the motionless state, which are a function of z only and are given in terms of asymptotic expansions for small δ as

$$\theta_B = (z - 1) + \delta(z - z^2)G/2 + \dots, \tag{3a}$$

$$\phi_B = \frac{\delta(1-z)}{C} + \delta^2\left[\frac{-(1-z)^2}{C^2} + \frac{(z^2-z)G}{2C}\right] + \dots, \tag{3b}$$

$$P_B = P_0 + R\left[(z - \tfrac{1}{2}z^2) + \delta(\tfrac{1}{2}z^2 - \tfrac{1}{3}z^3)\tfrac{1}{2}G + \dots\right], \tag{3c}$$

where $G \equiv 1 + S/C$ and P_0 is a constant. Since ϕ is small, the following expansion for $K(\tilde{\phi})$ is considered:

$$K(\tilde{\phi}) = 1 + K_1\tilde{\phi} + K_2\tilde{\phi}^2 + \dots, \tag{4}$$

where K_1 and K_2 are constants.

For the analysis presented in the next section, it was found to be convenient to use the general representation

$$\boldsymbol{u} = \boldsymbol{\Omega}V + \boldsymbol{E}\Psi, \quad \boldsymbol{\Omega} \equiv \nabla \times \nabla \times \boldsymbol{z}, \quad \boldsymbol{E} \equiv \nabla \times \boldsymbol{z}, \tag{5}$$

for the divergent-free vector field $\boldsymbol{u}$ (Chandrasekhar1961), where V and Ψ are the poloidal and toroidal functions for $\boldsymbol{u}$, respectively. By taking the vertical component of the curl of $(1a)$, it can be shown that the toroidal part $E\Psi$ of $\boldsymbol{u}$ must vanish. Taking the vertical component of the double curl of $(1a)$ and using $(1b)$ and (5) in (1), we find the final version of the governing system:

$$\nabla^2[K(\phi_B + \varepsilon\phi)\Delta_2 V] + \frac{\partial}{\partial z}[\boldsymbol{\Omega} V \cdot \nabla K(\phi_B + \varepsilon\phi)] - R\Delta_2\theta = 0, \tag{6a}$$

$$\left(\frac{\partial}{\partial t} - \delta\frac{\partial}{\partial z}\right)\left(-\theta + \frac{S\phi}{\delta}\right) + R\left(\frac{\mathrm{d}\theta_B}{\mathrm{d}z}\right)\Delta_2 V + \nabla^2\theta = \varepsilon R\boldsymbol{\Omega} V \cdot \nabla\theta, \tag{6b}$$

$$\left(\frac{\partial}{\partial t} - \delta\frac{\partial}{\partial z}\right)\left[(-1 + \phi_B)\theta + \theta_B\phi + \varepsilon\phi\theta - \frac{C\phi}{\delta}\right] + R\left(\frac{\mathrm{d}\theta_B}{\mathrm{d}z}\right)\Delta_2 V = \varepsilon R\boldsymbol{\Omega} V \cdot \nabla\theta, \tag{6c}$$

$$\theta = V = 0 \quad \text{at} \quad z = 0, \tag{6d}$$

$$\theta = V = \phi = 0 \quad \text{at} \quad z = 1, \tag{6e}$$

where

$$\Delta_2 \equiv \frac{\partial^2}{\partial x^2} + \frac{\partial^2}{\partial y^2}.$$

3. Analysis

In this section we first carry out a weakly nonlinear analysis, based on double-series expansions in powers of δ and ε, to determine the finite-amplitude simple (non-mixed) and mixed oscillatory and steady solutions and then investigate the stability of such solutions. As in the finite-amplitude analysis carried out in part 1, we first make a formal asymptotic expansion in ε and then at each order in ε make a formal asymptotic expansion in δ. Since we investigate both steady and oscillatory modes of convection, the appropriate expansions are for the dependent variables of the perturbation system (1), R and the frequency ω for the oscillatory modes of convection. These expansions are already provided in part 1 but will be given briefly below to make the present paper more self-contained for the reader:

$$\begin{aligned} &(V, \theta, \phi, R, \omega) \\ &= [(V_{00} + \delta V_{01} + \ldots.), (\theta_{00} + \delta\theta_{01} + \ldots.), (\phi_{00} + \delta\phi_{01} + \ldots.), \\ &\quad (R_{00} + \delta R_{01} + \ldots.), (\omega_{00} + \delta\omega_{01} + \ldots.)] + \varepsilon[(V_{10} + \delta V_{11} + \ldots.), \\ &\quad (\theta_{10} + \delta\theta_{11} + \ldots.), (\phi_{10} + \delta\phi_{11} + \ldots.), (R_{10} + \delta R_{11} + \ldots.), \\ &\quad (\omega_{10} + \delta\omega_{11} + \ldots.)] + \varepsilon^2[(V_{20} + \delta V_{21} + \ldots), (\theta_{20} + \delta\theta_{21} + \ldots), \\ &\quad (\phi_{2(-1)}/\delta + \phi_{20} + \delta\phi_{21} + \ldots), (R_{20} + \delta R_{21} + \ldots), (\omega_{20} + \delta\omega_{21} + \ldots)] + \ldots, \end{aligned} \tag{7}$$

where, as in the case of simple modes (Anderson & Worster 1995; part 1), the expansion of ϕ is singular at order ε^2 as $\delta \to 0$, but it turns out that $O(1/\delta)$ is needed only in the stability analysis to be presented later in this section since the $O(\varepsilon^2)$ problem is found to be forced by a term of $O(1/\delta)$ in the solute equation for the disturbances.

3.1. *Linear problem*

Upon inserting (4) and (7) into $(1a)$–$(1e)$ and disregarding the nonlinear terms, we find the linear problem, the analysis of which for the oscillatory modes (part 1) was done in direct analogy to that carried out by Anderson & Worster (1995) for the

stationary modes. Hence, no details will be provided here and, instead, the main results on the neutral boundary are given below first for the oscillatory modes and then for the stationary modes.

We consider first the oscillatory modes for the linear problem. At order $1/\delta$ we find $\omega_{00} = 0$. At order δ^0 we find

$$V_{00}^{(o)} = \left\{ \frac{\pi^2 + \left(a^{(o)}\right)^2}{R_{00}^{(o)} \left(a^{(o)}\right)^2 G} \right\} \sin(\pi z) \sum_{m=-M}^{M} (A_m^+ \eta_m^+ + A_m^- \eta_m^-), \tag{8a}$$

$$\theta_{00}^{(o)} = -\sin(\pi z) \sum_{m=-M}^{M} (A_m^+ \eta_m^+ + A_m^- \eta_m^-), \tag{8b}$$

$$\phi_{00}^{(o)} = \sum_{m=-M}^{M} [f_m(z) A_m^+ \eta_m^+ + f_m^*(z) A_m^- \eta_m^-], \tag{8c}$$

where

$$\eta_m^\pm \equiv \exp\left[i\left(\boldsymbol{a}_m^{(o)} \cdot \boldsymbol{r} \pm S_m \omega_{01} t\right)\right], \tag{8d}$$

$$R_{00}^{(o)} = \left\{ \frac{\left[\pi^2 + \left(a^{(o)}\right)^2\right]^2}{\left(a^{(o)}\right)^2 G} \right\}^{0.5}, \tag{8e}$$

$$f_m(z) = \left\{ \frac{-2\pi^3}{CG\left(\pi^2 - \omega_{01}^2\right)} \right\} \left\{ i\frac{\omega_{01} S_m}{\pi} \sin(\pi z) + \cos(\pi z) + \exp[i\omega_{01} S_m(z-1)] \right\} \tag{8f}$$

and

$$S_m = 1 \quad \text{for} \quad m > 0 \quad \text{and} \quad -1 \quad \text{for} \quad m < 0. \tag{8g}$$

Here the quantities with a superscript 'o' represent those for the oscillatory modes, i is the pure imaginary number ($i \equiv \sqrt{-1}$), subscript 'm' takes only non-zero integer values from $-M$ to M, M is a positive integer, $\boldsymbol{r}$ is the position vector, and the horizontal wavenumber vectors $\boldsymbol{a}_m^{(o)}$ satisfy the properties

$$\boldsymbol{a}_m^{(o)} \cdot \boldsymbol{z} = 0, \quad \left|\boldsymbol{a}_m^{(o)}\right| = a^{(o)}, \quad \boldsymbol{a}_{-m}^{(o)} = -\boldsymbol{a}_m^{(o)}. \tag{9}$$

The coefficients A_m^+ and A_m^- satisfy the conditions

$$\sum_{m=-M}^{M} (|A_m^+|^2 + |A_m^-|^2) = 2, \quad A_m^{\pm *} = A_{-m}^{\pm}, \tag{10}$$

where the asterisk indicates the complex conjugate. Minimizing the expression for $R_{00}^{(o)}$ given in (5d), with respect to the wavenumber $a^{(o)}$, we find

$$R_{00c}^{(o)} = \frac{2\pi}{\sqrt{G}}, \quad a_c^{(o)} = \pi. \tag{11}$$

We now consider the stationary modes for the linear problem. At the lowest order δ^0 we find

$$V_{00}^{(s)} = \frac{1}{\pi \sqrt{G}} \sin(\pi z) \sum_{n=-N}^{N} (A_n \eta_n), \tag{12a}$$

$$\theta_{00}^{(s)} = -\sin(\pi z) \sum_{n=-N}^{N} (A_n \eta_n), \tag{12b}$$

$$\phi_{00}^{(s)} = \frac{-2\pi}{CG}[1 + \cos(\pi z)] \sum_{n=-N}^{N} (A_n \eta_n), \tag{12c}$$

$$R_{00}^{(s)} = \left\{ \frac{[\pi^2 + (a^{(s)})^2]^2}{(a^{(s)})^2 G} \right\}^{0.5}, \tag{12d}$$

where

$$\eta_n \equiv \exp(\mathrm{i} \boldsymbol{a}_n^{(s)} \cdot \boldsymbol{r}). \tag{12e}$$

Here the quantities with a superscript 's' represent those for the stationary modes, subscript 'n' takes only non-zero integer values from $-N$ to N, N is a positive integer, and the horizontal wavenumber vectors $\boldsymbol{a}_n^{(s)}$ satisfy the properties

$$\boldsymbol{a}_n^{(s)} \cdot \boldsymbol{z} = 0, \quad |\boldsymbol{a}_n^{(s)}| = a^{(s)}, \quad \boldsymbol{a}_{-n}^{(s)} = -\boldsymbol{a}_n^{(s)}. \tag{13}$$

The coefficients A_n satisfy the conditions

$$\sum_{n=-N}^{N} |A_n|^2 = 1, \quad A_n^* = A_{-n}. \tag{14}$$

Minimizing the expression for $R_{00}^{(s)}$, given in (9d), with respect to the wavenumber $a^{(s)}$, we find

$$R_{00c}^{(s)} = \frac{2\pi}{\sqrt{G}}, \quad a^{(s)} = \pi. \tag{15}$$

At order δ we find the solutions $V_{01}^{(o)}$, $\theta_{01}^{(o)}$, $\phi_{01}^{(o)}$, $V_{01}^{(s)}$, $\theta_{01}^{(s)}$ and $\phi_{01}^{(s)}$. The solvability condition at this order for the system of the oscillatory modes yields an expression for $R_{01}^{(o)}$ and an equation involving ω_{01}, which are both given by Anderson & Worster (1996) and will not be repeated here. Similarly, the solvability condition at this order for the system of the stationary modes yield an expression for $R_{01}^{(s)}$, which is also given by Anderson & Worster (1996) and also will not be repeated here. The critical $R_c^{(o)}$ and $R_c^{(s)}$ for the onset of oscillatory and stationary convection, to order δ^2, can then be written as

$$R_c^{(o)} = \frac{2\pi}{\sqrt{G}} + \delta R_{01}^{(o)} + O(\delta^2), \quad R_c^{(s)} = \frac{2\pi}{\sqrt{G}} + \delta R_{01}^{(s)} + O(\delta^2). \tag{16}$$

For later reference, we designate the critical value of R at the onset of experimentally observed mixed convection by R_c.

It turns out, as will be presented and discussed later in this paper, that for all the values of the parameters investigated so far, the critical values $R_c^{(o)}$ and $R_c^{(s)}$ of R for the oscillatory and stationary modes, respectively, always satisfy the condition

$$R_c^{(o)} < R_c^{(s)}, \tag{17}$$

and the difference $(R_c^{(s)} - R_c^{(o)})$ is small and decreases with decreasing $G_t \equiv (G - 1)/(CG^2)$. Following Busse & Riahi (1988) and in the limit of sufficiently small G_t, we superimpose the most critical stationary solution on the most critical oscillatory solution in the order δ^0. Hence, at order 'δ^0' we have the following mixed solution:

$$(V_{00}, \theta_{00}, \phi_{00}) = [V_{00}^{(o)}, \theta_{00}^{(o)}, \phi_{00}^{(o)}] + B[V_{00}^{(s)}, \theta_{00}^{(s)}, \phi_{00}^{(s)}], \tag{18}$$

where B is an arbitrary constant. The constant B can be thought of as a relative measure between the order-one amplitudes of the stationary and oscillatory modes at

the leading order of the perturbation analysis. Consistent with the conditions and the results given in (9), (11), (13) and (15), the present theory takes into account mixed stationary and oscillatory modes of convection, where the wavenumber vectors of the oscillatory modes are those of the stationary modes. Consequently, $M = N$ and $a_n^{(o)} = a_n^{(s)}$ for each n, and thus for simplicity of notation the wavenumber vector for each mode 'n' is designated, hereafter, by a_n. The motivation for considering equation (18) in the present analysis is to take into account the effect of both stationary and oscillatory modes and their subsequent nonlinear interactions on the resulting flow features and the preferred solutions.

3.2. *Nonlinear problem at* $O(\varepsilon)$

Next, we analyse the nonlinear problem for the governing system (6) at order ε. At order ε/δ, we find $\omega_{00} = 0$. At order ε the system (6a)–(6e) can be reduced to the form given by (A1) in the Appendix. To form the solvability conditions for the nonlinear system, we need to define the following two sets of special solutions of the linear system:

$$\left(V_{00n}^{(o)}, \theta_{00n}^{(o)} \right) = \left[\frac{1}{\pi\sqrt{G}}, -1 \right] \sin(\pi z)(A_n^+ \eta_n^+ + A_n^- \eta_n^- + \text{c.c.}), \qquad (19a)$$

$$\left(V_{00n}^{(s)}, \theta_{00n}^{(s)} \right) = \left[\frac{1}{\pi\sqrt{G}}, -1 \right] \sin(\pi z)(A_n \eta_n + \text{c.c.}), \qquad (19b)$$

where 'c.c.' indicates complex conjugate of the preceding expression. There is no need to consider special linear solutions for ϕ since it was possible to reduce the governing nonlinear system to a form where only (19) will be needed to form the necessary solvability conditions. This is because the thermal and solutal fields are decoupled to the leading order in both ε and δ.

The governing equations at order ε that will be used to form the necessary solvability conditions consist of the equation for the poloidal component of u and the reduced temperature equation, which is the equation resulted from eliminating the dependent variable for the solid fraction between the original temperature equation and the equation for the solute concentration. The solvability conditions are then obtained by multiplying the equation for the poloidal velocity at order ε by $GV_{00n}^{(o)}$ ($GV_{00n}^{(s)}$), the reduced temperature equation at order ε by $\theta_{00n}^{(o)}$ ($\theta_{00n}^{(s)}$), adding, applying the boundary conditions, averaging over the whole layer and taking a time average over period $2\pi/\omega_{01}$. This yield two sets of equations, which are reduced to those given by (A 2a) and (A 2b) in the Appendix. In these equations an angular bracket indicates the average over the layer. The systems (A 2a) and (A 2b) contain four types of integral expressions of the form $\langle \eta_n E_l E_p \rangle$, which differ from zero only if

$$a_n + a_l + a_p = 0 \qquad (20a)$$

and

$$e_l S_l + e_p S_p = 0, \qquad (20b)$$

where for each $q(q = l, p)$, E_q designates either η_q^+ with $e_q \equiv 1$ or η_q^- with $e_q \equiv -1$. The system (A 2b) also contains an integral expression of the form $\langle \eta_n \eta_l \eta_p \rangle$, which differs from zero only if (20a) holds.

The equations (A 2a) and (A 2b) under the conditions (20a) and (20b) are found to be satisfied in the cases of participating stationary modes alone or mixed modes where the convection is in the form of a hexagonal pattern or a superposition of hexagonal

patterns (Busse 1967), while the condition (20) cannot be satisfied for convection in the form of two-dimensional rolls, squares and rectangles.

Using (20), (A 2a) and (A 2b) are simplified. We have detected two major new classes of solutions for which R_{10} is non-zero and can represent one class of subcritical convection cases, where $\varepsilon R_{10} < 0$, and one class of supercritical convection cases, where $\varepsilon R_{10} > 0$. The analysis and the solutions for these classes are presented in the next sub-sections.

Before analysing the solutions for the mixed modes, it is constructive to describe briefly here the simple solutions for either a steady mode alone or an oscillatory mode alone as well as the main features of the mixed solutions. A simple steady solution for the flow variables of the convection problem can be in the form of steady cells in the horizontal plane. The regular steady cells can be in the form of steady two-dimensional rolls, steady rectangles and steady hexagons, and they are stationary in the space and independent with respect to time (Busse 1989). A simple oscillatory solution for the flow variables of the convection problems can be in the form of either standing wave cells or travelling wave cells in the horizontal plane. The regular standing wave cells can be in the form of standing rolls, standing rectangles and steady hexagons, and they are stationary in space just like steady cells. However, unlike steady cells, the amplitudes of the standing wave cells oscillate in time. The regular travelling wave cells can be in the form of travelling rolls, travelling rectangles and travelling hexagons, and they travel in space and oscillate in time. Distinguishing features of the mixed solutions are their behaviour in time and space, which are a superposition of that due to the steady and oscillatory modes that form these mixed solutions.

Simple travelling wave–steady mixed classes of modes

We consider the simple travelling component of the mixed solutions to be in the form of right-travelling modes where the phase velocity of each mode is in the direction of the component of the mode's wave vector along $\boldsymbol{r}$. When the simple travelling component of the mixed solutions is in the form of left-travelling modes where the phase velocity of each mode is in the direction opposite to that of the component of the mode's wave vector along $\boldsymbol{r}$, we find identical results for the value of the coefficients R_{10} and R_{20} for each detected solution. Hence, the analysis in this paper for the simple travelling component of the mixed solutions is presented only in the form of right-travelling modes. The right-travelling-steady mixed solutions of (A 2a) and (A 2b) under the conditions (20a) and (20b) are simplified and considered in the so-called 'semi-regular' case, where

$$|A_1^+| = \cdots = |A_N^+| = 0, \quad |A_1^-|^2 = \cdots = |A_N^-|^2 = 1/N, \quad |A_1|^2 = \cdots = |A_N|^2 = 1/(2N),$$
(21)

and the scalar product between any one of the $\boldsymbol{a}$-vectors and its two neighbouring $\boldsymbol{a}$-vectors takes the constant values α_1 and α_2 (Busse 1967; part 1). We then considered new types of mixed solutions with non-zero R_{10}, which turn out to be either regular solutions in the form of hexagons where $\alpha_1 = \alpha_2$ or more general solutions such as the superposition of mixed hexagonal solutions, but these more general solutions are expected to be unstable (Busse 1967). To describe the mixed hexagonal solutions, we write a simplified version of (A 2a) and (A 2b) in the form

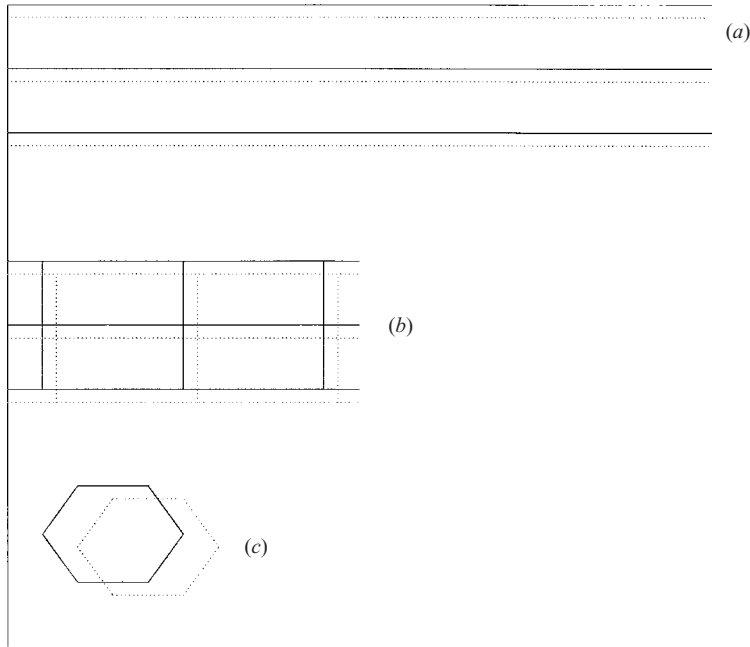$$R_{10} = C_1^{(j)} B, \quad R_{10} B = C_2^{(j)} + C_3^{(j)} B^2,$$
(22)

FIGURE 1. Sketch of basic mixed cells in the form of (*a*) mixed rolls, (*b*) mixed rectangles and (*c*) mixed hexagons. The solid line presents a steady cell, and the dotted line presents either a standing cell at all times or travelling cell at an instant in time only.

where the coefficients $C_i^{(j)}$ ($i = 1, 2, 3$), which are functions of C, G, K_1 and ω_{01}, are considered here with $j = 1$ for these solutions. As was discussed earlier, depending on the sign of εR_{10}, these solutions, which are called here solution 1, can be either subcritical or supercritical. The expressions for the coefficients $C_i^{(1)}$ are given by (A3). The detected mixed solutions are called simple travelling hexagons–steady hexagons. They correspond to the case $N = 3$. Figure 1(*c*) presents a sketch of a mixed hexagonal cell where the solid line represents the stationary cell and the dotted line represents the simple travelling cell at an instant in time. Using (22), we find

$$\left[R_{10}^{(1)}\right]^2 = \frac{C_2^{(1)}\left(C_1^{(1)}\right)^2}{C_1^{(1)} - C_3^{(1)}}, \quad B = \frac{R_{10}^{(1)}}{C_1^{(1)}}. \tag{23a,b}$$

Standing wave–steady mixed class of modes

We now consider the oscillatory component of the mixed solutions in the form of standing waves where $A_n^+ = A_n^-$ for every n. The standing wave–steady mixed solutions of (A 2*a*) and (A 2*b*) subject to (20*a*) and (20*b*) are simplified and considered in the semi-regular case, where

$$|A_1^\pm|^2 = \cdots = |A_N^\pm|^2 = 1/(2N), \quad |A_1|^2 = \cdots = |A_N|^2 = 1/(2N). \tag{24}$$

Just as in the case of the simple travelling wave–steady mixed class of solutions, we considered mixed and regular solutions in the form of hexagons for which (22) hold, where the coefficients $C_i^{(j)}$ ($i = 1, 2, 3$) are now considered with $j = 2$ for these solutions, which are called here solution 2. These solutions are the same as those for the simple travelling wave–steady mixed solutions, provided the simple travelling component is replaced by the standing wave component. The result (23) holds here,

with the superscripts '1' replaced by superscripts '2', where the expressions for $C_i^{(2)}$ are given by (A4). Figure 1(*c*) presents a sketch of a standing wave–steady hexagonal cell, where the solid line represents the steady cell, while the dotted line represents the standing cell at all times.

General travelling wave–steady mixed class of modes

We consider the oscillatory component of the mixed solutions to be in the form of general travelling waves of the types introduced in part 1. The general travelling–steady mixed solutions of (A 2*a*) and (A 2*b*) subject to (20*a*) and (20*b*) are simplified and considered in the semi-regular case, where

$$|A_1^+| = \cdots = |A_N^+| = [(0.5 - b)/N]^{0.5}, \quad |A_1^-| = \cdots = |A_N^-| = [(0.5 + b)/N]^{0.5},$$
$$|A_1| = \cdots = |A_N| = 1/(2N), \tag{25a}$$

and the constant b, restricted to

$$|b| < 0.5 \tag{25b}$$

(part 1), is the parameter for the general travelling component, when restricted to the range (25*b*) and the normalization condition given in (10), provides the particular general travelling component of the mixed solutions.

Similar to the case of the simple travelling wave–steady mixed class of modes described before, we considered mixed and regular solutions in the form of hexagons for which (22) hold, where the coefficients $C_i^{(j)}$ ($i = 1, 2, 3$) are now considered, with $j = 3$ for these solutions, which are called here solution 3. The description of solution 3 is the same as those for solutions 1 and 2 presented before, provided the simple travelling or standing component for the solutions is replaced by general travelling component. The result (23) holds here for these solutions, with the superscripts '1' replaced by superscripts '3'. The expressions for $C_i^{(3)}$ ($i = 1, 2, 3$) are given by (A5). Figure 1(*c*) presents a sketch of a simple or general travelling wave–steady mixed hexagonal cell, where the solid line represents the steady cell, while the dotted line can represent the travelling wave cell at an instance in time.

Solution to the governing system at $O(\varepsilon)$

The system of equations and boundary conditions at order ε are given by (A1). The solutions V_{10}, θ_{10} and ϕ_{10} of this system, which will be needed for the analysis of the governing system at $O(\varepsilon^2)$ to be presented in the next subsection, are found by first solving (A 1*a*) and (A 1*b*) for V_{10} and θ_{10} and then using these in (A 1*c*) to find ϕ_{10}, and are given in a supplement to the online version of the paper, (also available from the author or JFM Editorial Office, Cambridge).

3.3. *Nonlinear problem at $O(\varepsilon^2)$*

The solvability conditions for the system at order ε^2/δ yield $\omega_{20} = 0$ and trivial (zero) solutions follow for the dependent variables. At order ε^2 the system (6*a*)–(6*e*) can be reduced to the form given by (A6). The solvability conditions for the system to the order ε^2 are obtained in direct analogy to those obtained for the order-ε system. This yields two sets of equations containing sixteen types of integral expressions of the form $\langle E_n E_m E_l E_p \rangle$, which differ from zero only if

$$\boldsymbol{a}_n + \boldsymbol{a}_m + \boldsymbol{a}_l + \boldsymbol{a}_p = 0 \tag{26a}$$

and

$$e_n S_n + e_m S_m + e_l S_l + e_p S_p = 0 \tag{26b}$$

hold, where for each q ($q = n$, m, l, p), E_q denotes either η_q^+ with $e_q \equiv 1$ or η_q^- with $e_q \equiv -1$. These two sets of equations also contain four types of integral expressions of the form $\langle \eta_n \eta_m E_l E_p \rangle$, which differ from zero only if (20b) and (26a) hold, and four types of integral expressions of the form $\langle \eta_n E_l E_p \rangle$, which differ from zero only if (20a) and (20b) hold. In addition, the set of equations describing the solvability conditions contains integral expressions either of the form $\langle \eta_n \eta_m \eta_l \eta_p \rangle$, which differ from zero only if (26a) holds, or of the form $\langle \eta_n \eta_l \eta_p \rangle$, which differ from zero only if (20a) holds. Using conditions (20a), (20b), (26a) and (26b) in the resulting solvability conditions, we obtain a simplified sets of equations, which are given by (A 7a) and (A 7b).

The systems (A 7a) and (A 7b), together with (10) and (14), can be used to study mixed solutions in the form of two-dimensional oscillatory rolls–steady rolls and three-dimensional non-hexagonal cells, while (10), (14), (23), (A 7a) and (A 7b) can be used to study mixed solutions in the form of oscillatory hexagons-steady hexagons. Since the simplest types of solutions are often observed in the applications, we shall restrict our attention here to the simplest types of mixed solutions, which are either regular or semi-regular, and depending on whether the oscillatory component of the mixed solution is a simple travelling wave, a standing wave or a general travelling wave, then (21), (24) or (25a) is satisfied.

To describe the simple form of the mixed solutions, we write (A 7a) and (A 7b) in the form

$$R_{20} = C_4^{(j)} + C_5^{(j)} B^2 + S \left(C_6^{(j)} \omega_{11} + C_7^{(j)} R_{10} \right) B, \left. \right\}$$
$$R_{20} B = C_8^{(j)} B + C_9^{(j)} B^3 + S \left(C_{10}^{(j)} \omega_{11} + C_{11}^{(j)} R_{10} \right) + C_{12}^{(j)} B^2, \left. \right\} \tag{27}$$

where the coefficients $C_i^{(j)}$ ($i = 4, \ldots, 12$), which are in general functions of C, S, K_1, K_2, ω_{01}, N and ψ_{nm}, are those for each of the j-solutions ($j = 1, \ldots, 12$) that we shall consider here. There is no need to list the expressions for these 108 coefficients since they are provided in (A 7a) and (A 7b), which are just a different form of those given in (27). Using (27), we find for non-hexagonal type solutions

$$R_{20}^{(j)} = \frac{C_5^{(j)} C_8^{(j)} - C_4^{(j)} C_9^{(j)}}{C_5^{(j)} - C_9^{(j)}}, \quad B = \left[\frac{R_{20}^{(j)} - C_4^{(j)}}{C_5^{(j)}} \right]^{0.5}, \tag{28a}$$

while for hexagonal solutions we have (24) and

$$R_{20}^{(j)} = \left\{ C_4 + \frac{\left(R_{10}^{(j)} \right)^2}{C_1^{(j)}} \frac{C_7^{(j)} + C_5^{(j)}}{C_1^{(j)}} - \frac{C_6^{(j)} \left(R_{10}^{(j)} \right)^2}{C_{10}^{(j)} C_1^{(j)}} \frac{C_8^{(j)} + C_{11}^{(j)} C_1^{(j)}}{C_1^{(j)}} - \frac{C_6^{(j)} C_9^{(j)}}{C_{10}^{(j)}} \left(\frac{R_{10}^{(j)}}{C_1^{(j)}} \right)^4 \right.$$
$$\left. - \frac{C_6^{(j)} C_{12}^{(j)}}{C_{10}^{(j)}} \left(\frac{R_{10}^{(j)}}{C_1^{(j)}} \right)^3 \right\} \Big/ \left[1 - \frac{C_6^{(j)}}{C_{10}^{(j)}} \left(\frac{R_{10}^{(j)}}{C_1^{(j)}} \right)^2 \right], \tag{28b}$$

$$\omega_{11}^{(j)} = \left[\left(R_{20}^{(j)} - C_8^{(j)} - C_{11}^{(j)} C_1^{(j)} \right) \frac{R_{10}^{(j)}}{C_1^{(j)}} - C_{12}^{(j)} \left(\frac{R_{10}^{(j)}}{C_1^{(j)}} \right)^2 - C_9^{(j)} \left(\frac{R_{10}^{(j)}}{C_1^{(j)}} \right)^3 \right] \Big/ C_{10}^{(j)}, \tag{28c}$$

where superscript 'j' represents solution number j. Here j runs from 1 to 12, for the 12 mixed solutions to be described briefly later in this subsection.

The simple form of regular and mixed types of solutions correspond to the cases of two-dimensional oscillatory rolls–steady rolls ($N = 1$), oscillatory squares–steady squares ($N = 2$) and oscillatory hexagons–steady hexagons ($N = 3$), while those for a semi-regular and mixed types of solution correspond to the cases of oscillatory rectangles–steady rectangles ($N = 2$) with different values of angle γ. Here,

γ $(0 < \gamma < 90°)$ or $180° - \gamma$ is the angle between any two adjacent wavenumber vectors of a rectangular cell for a particular solution in the form of rectangles.

The simplest types of mixed solutions, which are found in the present study to be preferred under certain restricted conditions, are described briefly as follows. For a mixed solution in the form of simple travelling rolls–steady rolls, (21) and (A 7a) and (A 7b) hold for $N - 1 = S = 0$, and such a solution has $j = 4$ in (28a). For a mixed solution in the form of standing rolls–steady rolls, (24) and (A 7a) and (A 7b) hold for $N - 1 = S = 0$, and such a has $j = 5$ in (28a). For a mixed solution in the form of general travelling rolls–steady rolls, (25a) and (A 7a) and (A 7b) hold for $N - 1 = S = 0$, and such a solution has $j = 6$ in (28a). Figure 1(a) presents a sketch of standing wave–steady mixed rolls, where the solid lines represent the steady rolls, while the doted lines represent the standing roll cells at all times. The same picture also represents simple or general travelling wave–steady mixed roll cells, where the solid line represents the steady rolls, while the dotted line represents the travelling roll cells at an instant in time only. For a mixed solution in the form of either simple travelling rectangles–steady rectangles ($\gamma \neq 90°$), where $j = 7$ in (28a), or simple travelling squares–steady squares ($\gamma = 90°$), where $j = 10$ in (28a), (21) and (A 7a) and (A 7b) hold for $N - 2 = S = 0$. For a mixed solution in the form of either standing rectangles–steady rectangles ($\gamma \neq 90°$), where $j = 8$ in (28a), or standing squares–steady squares ($\gamma = 90°$), where $j = 11$ in (28a), (24) and (A 7a) and (A 7b) hold for $N - 2 = S = 0$. For a mixed solution in the form of either general travelling rectangles–steady rectangles ($\gamma \neq 90°$), $j = 9$ in (28a), or general travelling squares–steady squares ($\gamma = 90°$), $j = 12$ in (28a), (25a) and (A 7a) and (A 7b) hold for $N - 2 = S = 0$. Figure 1(b) presents a sketch of particular standing wave-steady mixed rectangular cells, where the solid lines represents the steady rectangles, while the dotted lines represent the standing wave cells at all time. The same picture also represents particular simple or general travelling wave–steady mixed rectangular cells, where the solid lines represent the steady rectangles, while the dotted lines represent the travelling wave cells at an instant in time only. For mixed subcritical (supercritical) solutions in the form of simple travelling hexagons–steady hexagons, where $j = 1$ in (23) and (28b) and (28c), equations (21) and (A 7a) and (A 7b) hold for $N = 3$ and $S = 1$, with $R_{10} < 0$ (>0) in the case of up-hexagons, while $R_{10} > 0$ (<0) in the case of down-hexagons. As will be referred to later in §4, the sign of the vertical motion at the cells' centres for the mixed hexagons, which is determined by the sign of ε, can be inferred from the condition

$$\varepsilon R_{10} < 0 \qquad\qquad (29a)$$

for the subcritical hexagons, which can be realized for $R < R_c$, and from the condition

$$\varepsilon R_{10} > 0 \qquad\qquad (29b)$$

for the supercritical hexagons, which can be realized for $R > R_c$.

For mixed solutions in the form of standing hexagons–steady hexagons, for which $j = 2$ in (23) and (28b)–(28c), (24) and (A 7a)–(A 7c) hold for $N = 3$ and $S = 1$. For mixed solutions in the form of general travelling hexagons-steady hexagons, for which $j = 3$ in (23) and (28b), (28c), (25a)–(25c) and (A 7a)–(A 7c) hold for $N = 3$ and $S = 1$. Figure 1(c) presents a sketch of a standing wave–steady mixed hexagonal cell, where the solid line represent the steady hexagon, while the dotted line represent the standing hexagonal cell at all time. The same picture also represents a simple or general travelling wave–steady mixed hexagonal cell, where the solid line represents the steady hexagon, while the dotted line represents the travelling hexagonal cell at

Solution	Stationary modes	Oscillating modes	N	$\gamma^{(\text{deg.})}$	$\lvert b \rvert$	R_{10}	R_{20}
1	steady hexagons	simple travelling hexagons	3	60	0.5	$\neq 0$	positive
2	steady hexagons	standing hexagons	3	60	0.0	$\neq 0$	positive
3	steady hexagons	general travelling hexagons	3	60	positive & less than 0.5	$\neq 0$	positive
4	steady rolls	simple travelling rolls	1	180	0.5	0	non-zero
5	steady rolls	standing rolls	1	180	0	0	non-zero
6	steady rolls	general travelling rolls	1	180	Positive & less than 0.5	0	non-zero
7	steady rectangles	simple travelling rectangles	2	positive & less than 90	0.5	0	non-zero
8	steady rectangles	standing rectangles	2	positive & less than 90	0	0	non-zero
9	steady rectangles	general travelling rectangles	2	positive & less than 90	positive & less than 0.5	0	non-zero
10	steady squares	simple traveling squares	2	positive & less than 90	0.5	0	non-zero
11	steady squares	standing squares	2	positive & less than 90	0	0	non-zero
12	steady squares	general travelling squares	2	positive & less than 90	positive & less than 0.5	0	non-zero

TABLE 1. The 12 mixed solutions and their main features.

an instant in time only. Table 1 presents a list of these twelve mixed solutions and their main features as determined in this paper.

3.4. *Stability problem*

The analysis of the nonlinear problem presented in §§ 3.2 and 3.3 has shown that an infinite manifold of solutions could exist even though this represents only an infinitesimal fraction of the manifold of the solutions (18) of the linear problem. To distinguish the physically realizable solutions from among all the possible mixed solutions, the stability of V, θ, ϕ with respect to arbitrary three-dimensional disturbances V_d, θ_d, ϕ_d should be investigated. The time-dependent disturbances can be assumed in the form

$$(V_d, \theta_d, \phi_d) = [V'(x, y, z, t), \theta'(x, y, z, t), \phi'(x, y, z, t)] \exp(\sigma t), \qquad (30)$$

where σ is the growth rate of the disturbances. When the governing equations and the boundary conditions of the form (6a)–(6e) for the finite-amplitude mixed flow are subtracted from the corresponding equations and boundary conditions for the total dependent variables for the mixed flow and the disturbance quantities, and the result-ing system is linearized with respect to the disturbance quantities, we obtain the stability system given by (A 8a)–(A 8e).

When expansion (7) is used in (A 8a)–(A 8e), it becomes evident that the stability system can be solved by a similar expansion. Hence, the disturbance variables ω' and the disturbance growth rate σ are expanded in a similar way to the corresponding perturbation variables in equation (7).

For the present stability analysis we consider the superposition of both stationary and oscillatory disturbances. For stationary disturbances, we restrict ourselves to those with dependent variables having wavenumber vectors $\boldsymbol{a}'_n$, which all have

wavenumbers $|\boldsymbol{a}'_n| = a' = a_c$. For oscillatory disturbances, we restrict ourselves to those with dependent variables having wave number vectors $\boldsymbol{a}'_n$ and frequencies ω'_n, which all have wavenumbers $|\boldsymbol{a}'_n| = a' = a_c$ and linear frequencies $\omega'_0 = \omega_c$, where

$$\omega'_0 = \omega'_{00} + \delta\omega'_{01} + \dots$$

and ω_c is the most critical frequency ω_{01} detected earlier for the linear problem for the oscillatory modes. Then the most critical disturbances, which have the maximum growth rate, are found to be characterized by $\sigma_0 = 0$, where

$$\sigma_0 = \sigma_{00} + \delta\sigma_{01} + \dots.$$

The linear solutions for the dependent variables of the disturbances at order δ^0 are found to be of the form (18), with A_n, $A_n^\pm$, η_n, $\eta_n^\pm$, B and N replaced, respectively, by arbitrary constants $\tilde{A}_n$, arbitrary constants $\tilde{A}_n^\pm$, $\tilde{\eta}_n = \exp(\mathrm{i}\boldsymbol{a}'_n \cdot \boldsymbol{r})$, $\tilde{\eta}_n^\pm = \exp[\mathrm{i}(\boldsymbol{a}'_n \cdot \boldsymbol{r} \pm S_n\omega'_n t)]$, constant $\tilde{B}$ and ∞.

In analogy to the solvability conditions for the mixed oscillatory–steady motion presented in §3.3, the solvability conditions for the disturbance systems at order $\varepsilon^n (n > 1)$ require us to define two independent particular solutions of the linear system for the disturbances. These solutions, designated either by $\tilde{V}_{00n}^{(o)}$ and $\tilde{\theta}_{00n}^{(o)}$ or by $\tilde{V}_{00n}^{(s)}$ and $\tilde{\theta}_{00n}^{(s)}$, have the same form as either (19a) or (19b), with $A_n^\pm$, $\eta_n^\pm$, A_n and η_n replaced, respectively, by $\tilde{A}_n^\pm$, $\tilde{\eta}_n^\pm$, $\tilde{A}_n$ and $\tilde{\eta}_n$. The solvability conditions for the disturbance systems at order ε and ε^2, which are needed to determine σ_{10} and σ_{20}, respectively, are derived similarly to the corresponding ones for the mixed flow system, which have already been described. The solvability conditions at orders ε and ε^2 yield very lengthy systems of equations for $\tilde{A}_n^\pm$, $\tilde{A}_n$, $\tilde{B}$, ω'_{11}, σ_{10} and σ_{20}, which will not be given here. The leading-order growth rate $\sigma^* = \varepsilon\sigma_{10} + \varepsilon^2\sigma_{20}$ of the disturbances acting on the finite-amplitude mixed motion can then be determined from these systems following the method of approach due to Busse (1967), which is now a standard stability procedure, both where the wavenumber vectors of the disturbances coincide with those of the mixed motion and where they do not.

4. Results and discussion

4.1. *Linear problem*

The linear system with eigenvalue problems for both oscillatory and stationary modes, which led to the results (8)–(19), are in general, functions of the two composite parameters G and G_t. As discussed in part 1, these two parameters, which can represent combinations of the scaled Stefan number S and the scaled compositional ratio C, are found to be relevant for the present mixed oscillatory–stationary system. Hence, the present results are provided for given values of G and G_t, instead of S and C. As explained earlier in §2, the present mixed system is most realistic for sufficiently small values of G_t. Note that for the experimental results due to Tait *et al.* (1992), their values are evaluated to be $G \approx 1.25$ and $G_t \approx 0.008$, so that G_t can be quite small experimentally. The results presented in this paper are relevant at least for the range of values $0.833 \leqslant S \leqslant 6.667$ and $3.333 \leqslant C \leqslant 26.667$, which correspond to $G = 1.25$ and $0.006 \leqslant G_t \leqslant 0.048$. The results for the frequency ω_{01} of the oscillatory component of the mixed solutions as function of small values of G_t $(0.006 \leqslant G_t \leqslant 0.048)$ are presented in figure 2. It turns out that ω_{01} is independent of K_1 and G. The results for $R_c^{(o)}$ and $R_c^{(s)}$ as functions of G_t and for given values $K_1 = 1.0$, $G = 1.25$ and $\delta = 0.2$ are given in figure 3. Similar to the calculation made in part 1, here the value of $\delta = 0.2$ is chosen to evaluate the critical values of the
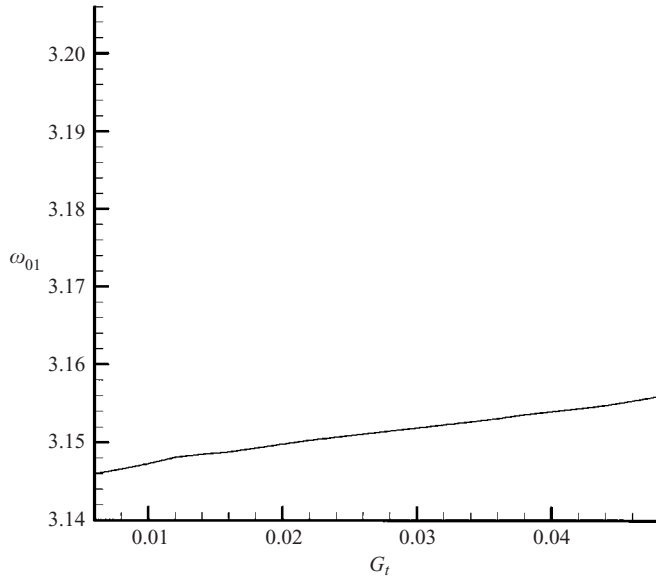
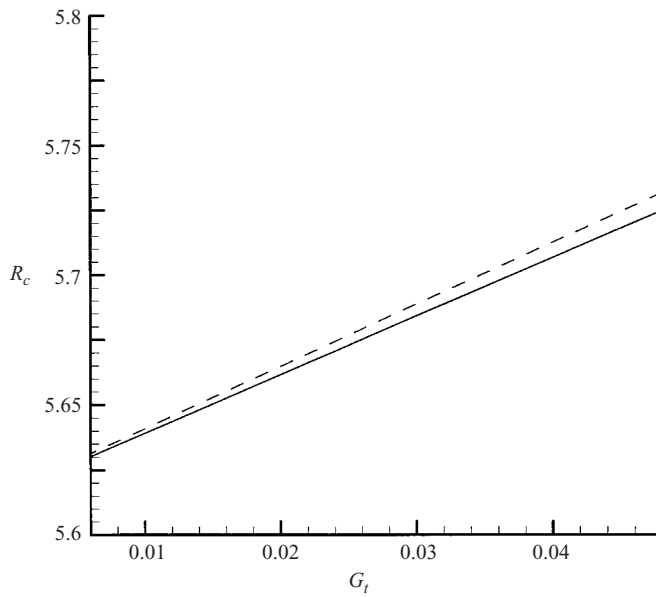FIGURE 2. The frequency ω_{01} versus G_t.

FIGURE 3. The critical values of the scaled Rayleigh numbers $R_c^{(o)}$ (solid line) and $R_c^{(s)}$ (dashed line) versus G_t for $G = 1.25$, $K_1 = 1.0$ and $\delta = 0.2$.

scaled Rayleigh number and other quantities whose values may depend on δ. It can be seen from figure 3 that both $R_c^{(o)}$ and $R_c^{(s)}$ are stabilizing with respect to G_t. The value of $R_c^{(o)}$ is consistently smaller than that for $R_c^{(s)}$ but $[R_c^{(s)} - R_c^{(o)}]$ decreases with decreasing G_t, and, as stated before, the present theory is most realistic in the range for G_t where $[R_c^{(s)} - R_c^{(o)}]$ is sufficiently small. For all G_t shown in figure 3 $[R_c^{(s)} - R_c^{(o)}]$ can be considered to be sufficiently small since its values are less than $1/500$ of either $R_c^{(s)}$ or $R_c^{(o)}$. Our additional calculations, as well as (16), indicated that both $R_c^{(o)}$ and
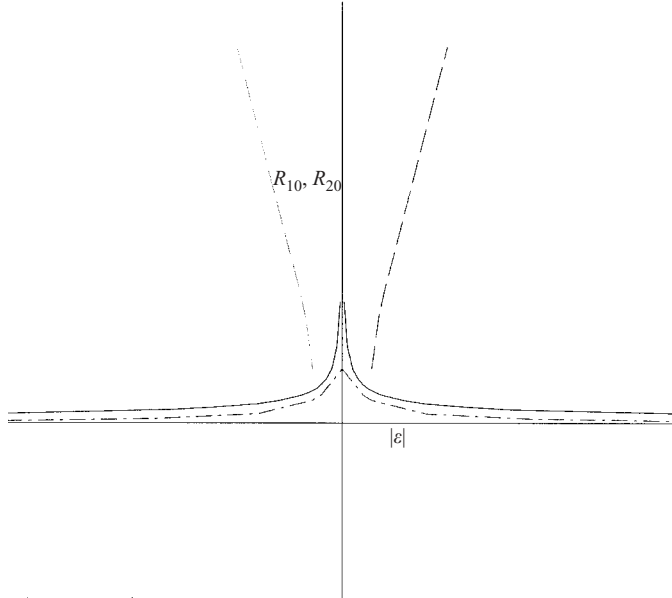
FIGURE 4. A qualitative sketch of $|\varepsilon|$ versus either R_{10} or R_{20} in the case of $R_{10}=0$ for the solutions with maximum order of magnitude of amplitude.

$R_c^{(s)}$ are destabilizing and stabilizing with respect to G and K_1, respectively, in the sense that both decrease with either increasing G or decreasing K_1. $[R_c^{(s)} - R_c^{(o)}]$ is, however, independent of K_1.

The physical meaning of the effects of G and G_t on the linear system is found to be the same as in the case of the stationary mode alone or the oscillatory mode alone, which was presented in part 1 and, hence, will not be repeated here. The stabilizing effect on the linear system when K_1 increases is consistent with the physical role played by K_1 since the permeability of the mushy layer decreases with increasing K_1.

4.2. Nonlinear problem

Important quantities due to the nonlinear effects are the coefficients R_{10} and R_{20}, which are calculated in the present study. As can be seen from the expansions (7), these coefficients represent leading contributions to the change in R required to obtain finite amplitude ε for a nonlinear solution. Figure 4 presents a qualitative sketch of the maximum of the order of magnitude $|\varepsilon|$ of the amplitude of convection either versus R_{10}, for a given R_{20}, in the case $\varepsilon R_{10} < 0$ (dashed lines) and in the case $\varepsilon R_{10} > 0$ (dashed-dot lines) or versus R_{20} in the case $R_{10}=0$ (solid lines). The graphs to the left of the $|\varepsilon|$-axis correspond to negative values of the respective coefficient R_{10} (or R_{20} in the case of $R_{10}=0$), while those to the right of the $|\varepsilon|$-axis correspond to positive values of the respective coefficient.

In agreement with the qualitative results presented in the figure 4, it should be noted that for non-zero R_{10}, which can correspond to the mixed solutions in the form of oscillatory hexagons–steady hexagons, then for the subcritical convection state where $R < R_c$, the amplitude of convection is largest when $|R_{10}|$ is largest, and for the supercritical convection where $R > R_c$, the amplitude of convection is largest when $|R_{10}|$ is smallest. For $R_{10}=0$, which corresponds to the mixed solutions in the form of oscillatory rolls–steady rolls, oscillatory squares–steady squares and oscillatory rectangles–steady rectangles, then the sign of R_{20} determines whether the

mixed solution exists for values of R above or below R_c. For $R_{10} = 0$ and supercritical convection, where $R > R_c$, the amplitude of convection is largest, provided R_{20} is smallest among all the mixed solutions to the nonlinear problem. In the present problem the coefficients R_{10} and R_{20} are due to the nonlinear convective terms in the temperature equation and the nonlinear interactions between the flow velocity and the non-uniform and nonlinear permeability associated with the perturbation to the basic-state solid fraction.

Oscillatory hexagons–steady hexagons

The coefficient R_{10}, given by (23), for solutions 1–3 ($j = 1, 2, 3$) in the form of simple travelling hexagons–steady hexagons, standing hexagons–steady hexagons and general travelling hexagons–steady hexagons, was computed for various values of G, G_t and K_1. It was found that for a given mixed solution, two values for R_{10} with the same magnitude but opposite sign are possible. The sign of εR_{10} determines whether the mixed solution exists for values of R above or below R_c. The convection due to mixed modes can be supercritical for (29b) and subcritical for (29a).

For the mixed solutions 1–3 where R_{10} is non-zero, it was found that the cell patterns, due to different joint oscillatory and stationary modes, referred to here as mixed patterns, behave like those of steady hexagons in the sense of contributing non-zero terms to the expression for R_{10}. For the supercritical case, up-hexagonal patterns, with up-flow at the cell centres and down-flow at the cell boundaries, correspond to the case where

$$\varepsilon > 0 \quad \text{and} \quad R_{10} > 0, \tag{31a}$$

while down-hexagonal patterns, with down-flow at the cell centres and up-flow at the cell boundaries, correspond to the case where

$$\varepsilon < 0 \quad \text{and} \quad R_{10} < 0. \tag{31b}$$

For subcritical case, up-hexagonal patterns correspond to the case

$$\varepsilon > 0 \quad \text{and} \quad R_{10} < 0, \tag{31c}$$

while down-hexagonal patterns correspond to the case

$$\varepsilon < 0 \quad \text{and} \quad R_{10} > 0. \tag{31d}$$

Here we are interested in studying the preferred mixed solutions 1–3, which, as to be shown later in this section, turn out to be stable, under some conditions, for sufficiently small $|\varepsilon|$ and correspond to the relatively lowest values of R. These types of mixed solutions satisfy either (31c) or (31d) and should correspond to the largest values of $|R_{10}|$.

Using (23), we calculated the values of R_{10} for the mixed solutions 1–3 for $G = 1.25$ but for different values of K_1 and G_t, where the experimentally relevant range of S and C referred to earlier in this section is covered. In all the calculations that were carried out, we found that $|R_{10}|$ increases with G_t and K_1 for each of these three mixed solutions, but $|R_{10}|$ has larger value for solution 2 in the form of standing hexagons–steady hexagons. It should be noted that (22) yields two solutions $\pm R_{10}$, provided the right-hand side of (23a) is positive, which was the case for the calculations that were carried out. The possibility of two solutions $\pm R_{10}$ to the present problem opens the possibility for the preference of subcritical down-mixed pattern and is in contrast to simple solutions in the form of either oscillatory modes alone (part 1), where no subcritical solution is possible, or stationary modes alone (Amberg & Homsy 1993), where no subcritical down-hexagons are possible.
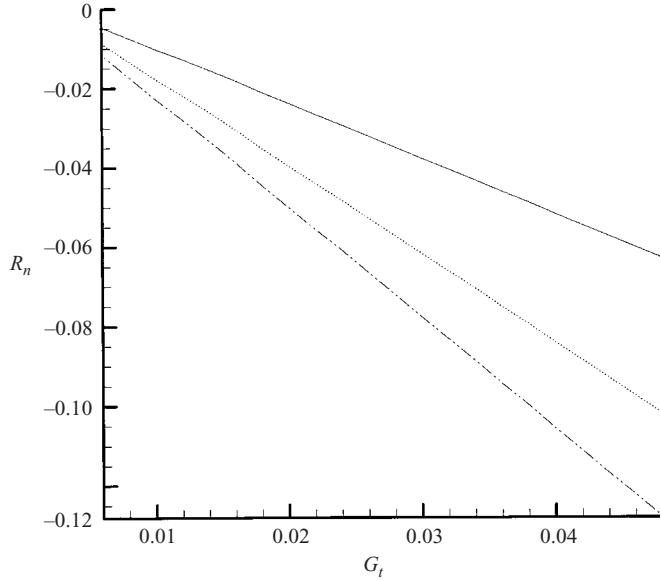
FIGURE 5. R_n versus G_t for subcritical flow in the form of standing down-hexagons–steady down-hexagons with $G = 1.25$ and $K_2 = 0$. Here the solid line, dotted line and dash-dot-dot line correspond to $K_1 = 0.005$, 0.008 and 0.01, respectively.

It is clear from the results based on the calculated values of R_{10} presented in the previous paragraph that solution 2 in the form of standing hexagons–steady hexagons is preferred over solutions 1 and 3. However, the results based on R_{10} alone do not distinguish between the subcritical up-hexagonal state and subcritical down-hexagonal state of solution 2 since each of these states corresponds to the same value of R_{10} for the same given parameter values. Hence, in order to determine which of these two states for solution 2 corresponds to the lower value of R, we need to inspect calculated values of the coefficient R_{20} given by (28b). Our generated data for R_{20} for the three solutions 1–3 and for different parameter values indicate that R_{20} is positive, increases with K_1 and K_2, and its values for solution 2 is consistently smaller than the corresponding values for solutions 1 and 3. However, although the coefficients R_{10} and R_{20} are important quantities in the present paper, the combined quantity $R_n = (\varepsilon R_{10} + \varepsilon^2 R_{20})/|\varepsilon| = (R - R_c)/|\varepsilon|$, which is valid to order up to and including ε^2 calculated in the present study, is the one that is of fundamental interest in the discussion of the results. Some typical results on the effects of G_t and K_1 are presented in figure 5 for R_n of the preferred solution 2 in the subcritical and down-hexagonal case ($R_{10} > 0$), which is designated by $R_n^{(dh)}$, for $G = 1.25$, $\varepsilon = -0.001$ and $K_2 = 0$. The destabilizing effect of K_1 and G_t on the subcritical state of solution 2 is apparent from the results presented in figure 5. We also calculated R_n for the preferred solution 2 in the subcritical and up-hexagonal case ($R_{10} < 0$), which is designated by $R_n^{(uh)}$, and found a similar trend and results for R_n in its variation with respect to the parameters, but the values of $R_n^{(dh)}$ for down-hexagonal case were found to be consistently smaller than the corresponding values for $R_n^{(uh)}$ for the up-hexagonal case. This important result is basically due to the cubic term in R_{10} in the numerator of the expression for R_{20} in (28b), which was found to be due to a nonlinear term contributed by the steady modes in the solvability condition (A 10b) for the order ε^2 system of the mixed solutions. It is found that ($R_n^{(uh)} - R_n^{(dh)}$) increases with K_1. Hence, the subcritical

down-hexagonal state of standing hexagons–steady hexagons appears to correspond to the smallest value of R. This result agrees with the experimental finding by Tait *et al.* (1992) that near the onset of motion the planform of compositional convection in a mushy layer is in the form of down-hexagons.

The solvability conditions for R_{20}, in the cases where R_{10} is non-zero, also lead to the result for a higher-order frequency correction ω_{11} given by (28c). For the preferred solution 2 in the form of standing hexagons–steady hexagons, we find that $\omega_{11} > 0$ for $R_{10} < 0$ and $\omega_{11} < 0$ for $R_{10} > 0$. The magnitude of ω_{11} increases slowly with G_t and K_1 and its order of magnitude is about 0.0001 for K_1 up to its present allowable value of about 0.01. Another point to note here is that in part 1, $R_{1n} = \omega_{1n} = 0$ ($n = 0, 1, \ldots$) due to the fact that horizontal averages $\langle \eta_n^\pm \eta_l^\pm \eta_p^\pm \rangle = 0$ because of the symmetry of the problem. However, in the present study R_{1n} and ω_{1n} are no longer zero for the hexagonal cases where asymmetry exists in the problem in the sense that a change in the sign of ε can lead to different types of solutions. This asymmetry in the present study is due to the stationary modes, where $\langle \eta_n \eta_l \eta_p \rangle \neq 0$ in general, and due to the interactions between the steady and oscillatory modes, where, for example, $\langle \eta_n \eta_l^\pm \eta_p^\pm \rangle \neq 0$ in general. The present nonlinear investigation is restricted to the range $K_1 \leqslant 0.01$ since for values of K_1 beyond this range, the absolute value of the coefficient R_{20} increases rapidly with K_1, becoming much larger than unity by about 2 orders of magnitude for K_1 just above 0.02, so that a modelling assumption of the type of (7), which assumes that the coefficients, such as $|R_{20}|$, in those double-expansions in powers of ε and δ be of order unity, can no longer be justified.

We also examined the vertical distribution of solid fraction at different times and locations in the horizontal direction for the preferred mixed solutions. Our data, generated over most of the periodic domain in time, at the centres and nodes of the preferred mixed solution in the form of standing hexagons–steady hexagons in the subcritical down-hexagonal state, indicated that even though the perturbation to the solid fraction at the nodes is positive in about the lower three-quarters of the layer, it is negative over about the upper quarter of the mushy layer. In addition, the sign of the perturbation to the solid fraction at the centres of the cells is generally opposite to that at the nodes. This general result holds irrespective of the parameter values considered, which indicates, in particular, that near the top of the layer, the tendency for chimney formation is higher at the nodes than at the centres. This result for the upper portion of the layer agrees with the experimental observation due to Tait *et al.* (1992) on chimney formation at the nodes of the down-hexagonal cells in a mushy layer. Some typical results are presented in figure 6 for the vertical distribution of the basic state (dotted line) and total solid fraction at both a centre (dashed line) and a node (solid line) of solution 2 in the subcritical down-hexagonal state, due to standing hexagons–steady hexagons. In these calculations $\delta = 0.2$, $G = 1.25$, $G_t = 0.008$, $K_1 = 0.005$, $K_2 = 0$, and the value $\varepsilon = -0.001$ is chosen, which corresponds to the maximum value of $|\varepsilon| = 0.001$ beyond which the solid fraction becomes negative. This is based on the physical grounds that the value of the perturbation to the solid fraction cannot be such that the total solid fraction becomes negative. It is seen from this figure that the tendency for chimney formation at the node is higher in the upper portion of the layer, but more at the centre over the rest of the layer. Similar to the discussion in part 1 for the solid fraction due to the standing modes, the chimneys and the compositional strips are in the vertical direction since the phase speed of these modes is zero, but the vertical extent of the chimneys can vary depending on the variation of the solid-fraction perturbation with respect to time. However, in the case of a mixed solution with a travelling-mode component, the chimneys and the
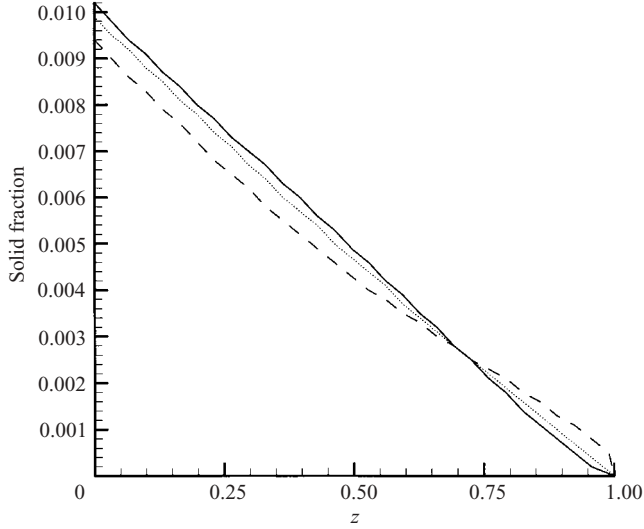
FIGURE 6. Solid fraction versus z for the preferred solution in the form of subcritical standing down-hexagons–steady down-hexagons with $\varepsilon = -0.001$ and $G = 1.25$, $G_t = 0.008$, $K_1 = 0.005$ and $K_2 = 0$. Here the dotted line, solid line and dashed line present the basic solid fraction ϕ_B, $\tilde{\phi}$ ($x = 1.33$, $y = 0$, $t = 0.5$) and $\tilde{\phi}$ ($x = y = 0$, $t = 0.5$), respectively.
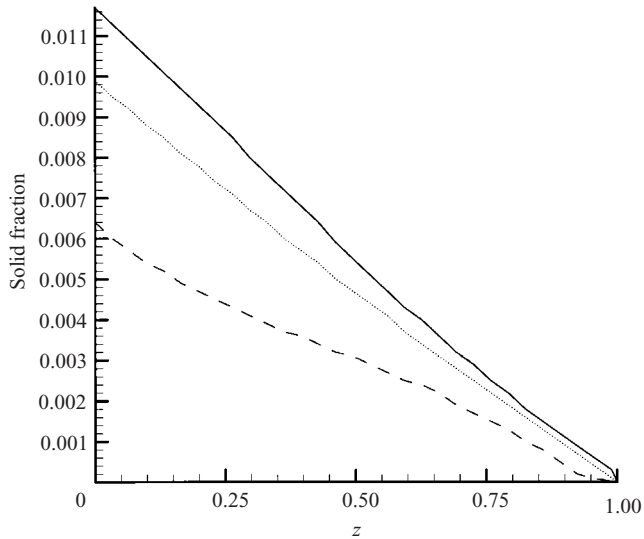

FIGURE 7. As figure 6 but for z for the preferred subcritical standing up-hexagons–steady up-hexagons with $\varepsilon = 0.001$.

compositional strips in a travelling wave state can be inclined because of the non-zero phase speed of such a wave relative to the uniform upward speed of the mushy layer (Anderson & Worster 1996; part 1). Figure 7 presents the results for the same parameter values as figure 6 but for $\varepsilon = 0.001$, so that the flow is upward at the cell centres and downward at the boundaries. It can be seen from the results presented in the figure 7 that here the tendency for the chimney formation is higher at the centres throughout the layer, while no such tendency exists at the node anywhere in the layer.

Oscillatory rolls–steady rolls

As was explained in the previous section, R_{10} is zero for mixed rolls. Thus, the important coefficient for rolls is R_{20} given by (28a) for solutions 4–6 ($j = 4, 5, 6$) in the form of simple travelling rolls–steady rolls, standing rolls–steady rolls and general travelling rolls–steady rolls, respectively. The coefficient R_{20}, designated $R_{20}^{(4)}$, $R_{20}^{(5)}$ and $R_{20}^{(6)}$ for solutions 4–6, respectively, was computed for various values of the parameters. As was the case for all solutions 1–12, the effect of K_2 was found to be stabilizing in the sense that R_{20} increases with K_2. However, the effect of K_1 on $R_{20}^{(4)}$, $R_{20}^{(5)}$ and $R_{20}^{(6)}$ was found to be destabilizing in the sense that these coefficients decrease with increasing K_1. In addition, it was found that the rate of increase of R_{20} with respect to K_2 is much smaller than the rate at which R_{20} decreases with increasing K_1. For the least stabilizing case where $K_2 = 0$, the main results on the coefficients $R_{20}^{(4)}$, $R_{20}^{(5)}$ and $R_{20}^{(6)}$ are as follows. $R_{20}^{(4)}$ is generally positive and, thus, the flow due to solution 4 is supercritical. $R_{20}^{(4)}$ is generally larger than either $R_{20}^{(5)}$ or $R_{20}^{(6)}$ for given parameter values and, thus, solution 4 is not preferred over solution 5 if $R_{20}^{(5)} > 0$ or over solution 6 if $R_{20}^{(6)} > 0$. As to be discussed later in this section, all the subcritical mixed solutions with $R_{10} = 0$ ($R_{20} < 0$) are found to be unstable and, therefore, such solutions are not preferred. However, only those supercritical mixed solutions with $R_{10} = 0$, which exhibits the smallest value of R_{20} for given parameter values, are found to be stable in a very restricted domain of the parameter values. It should be noted that solution 6 corresponds to a class of solutions in the form of general travelling rolls–steady rolls, which depends on the parameter b in the range (25b). Both $R_{20}^{(5)}$ and $R_{20}^{(6)}$ decrease rapidly with increasing K_1 and can become negative for K_1 above some values, which may depend on G_t if K_1 is sufficiently small. Thus subcritical solutions 5 and 6 are possible for K_1 above some small values. For example, $R_{20}^{(6)}$ for $b = 1.0$ is negative for $K_1 \geqslant 0.003$ over the whole range of G_t considered in this paper, it becomes negative for $K_1 = 0.002$ if $G \leqslant 0.034$, but it is positive over the whole range of G_t for $K_1 \leqslant 0.001$. However, $R_{20}^{(5)}$ is negative for $K_1 \geqslant 0.004$ over the whole range of G_t, it becomes negative for $K_1 = 0.003$ if $G_t \leqslant 0.042$ and for $K_1 = 0.002$ if $G_t \leqslant 0.016$, but it is positive over the whole range of G_t for $K_1 \leqslant 0.001$. Thus, for certain values of K_1 and G_t, the values of either $R_{20}^{(5)}$ or $R_{20}^{(6)}$ are very small and positive, and either solution 5 or solution 6 with the smaller value of R_{20} can become preferred over the other solution. It can be seen that supercritical solution 5 or supercritical solution 6 can be realized over a very small range in the (G_t, K_1)-plane.

Figure 8 presents the transition boundary between subcritical and supercritical regimes for solution 5 with different values of K_2 in the (G_t, K_1)-plane. The solution in the form of standing rolls–steady rolls is supercritical in the region below the curve for given K_2 in figure 8, and subcritical above. Thus, just below the curve for given K_1, G_t and K_2, the solution has very small positive value of $R_{20}^{(5)}$ and may be preferred. The results shown in this figure also indicate the general feature of a rather slow rate of stabilizing effect exerted by K_2 on the flow.

Oscillatory rectangles–steady rectangles

Here we consider mixed rectangular solutions 7–12, which include the classes of solutions with $\gamma \neq 90°$ (solutions 7–9) and the mixed squares with $\gamma = 90°$ (solutions 10–12). Again, as in the case of mixed rolls, $R_{10} = 0$ for such solutions. Thus, the important coefficient is R_{20} given by (28a) for solutions 7–12 ($j = 7, \ldots, 12$) designated by $R_{20}^{(7)}$, $R_{20}^{(8)}$, $R_{20}^{(9)}$, $R_{20}^{(10)}$, $R_{20}^{(11)}$ and $R_{20}^{(12)}$ respectively, was computed for each of these solutions for various values of the parameters. The effect of K_1 on all of these
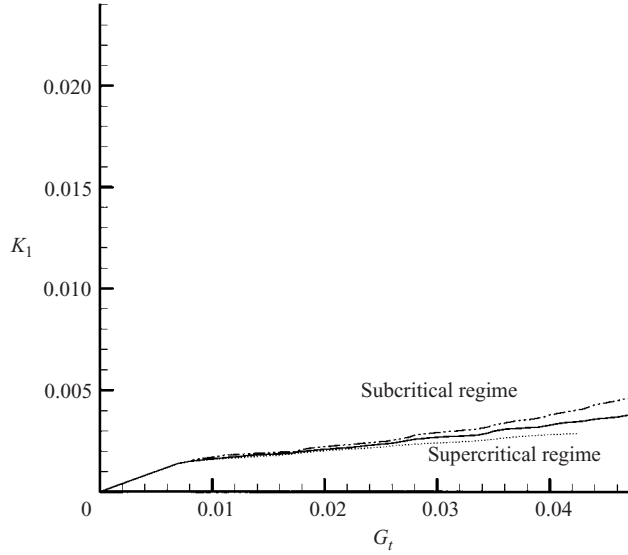
FIGURE 8. The transition boundary between subcritical and supercritical regimes for standing rolls–steady rolls in the (G_t, K_1)-plane with $G = 1.25$. Here the dotted line, solid line and dash-dot-dot line present the cases of $K_2 = 0$, 0.2 and 0.4, respectively.

coefficients was found to be destabilizing, so that their values decrease with increasing K_1. For the least stabilizing case where $K_2 = 0$, the main results for these coefficients are as follows. $R_{20}^{(7)}$ and $R_{20}^{(10)}$ are generally positive and, thus, the flows due to solutions 7 and 10 are supercritical. $R_{20}^{(10)}$ is generally larger than any of the other five coefficients for given parameters values, thus solution 10 is not preferred over any of the other five solutions, which may have a positive R_{20} value. It should also be noted that solutions 7–9 and 12 correspond to classes of solutions for either different values of b or different values of the angle γ for the mixed rectangular cases. $R_{20}^{(8)}$, $R_{20}^{(9)}$, $R_{20}^{(11)}$ and $R_{20}^{(12)}$ decrease rapidly with increasing K_1 and can become negative for K_1 beyond some values, which may depend on G_t if K_1 is sufficiently small. Thus, the subcritical state for solutions 8, 9, 11 and 12 is possible for K_1 above some small values. For example, $R_{20}^{(11)}$ is negative for $K_1 \geqslant 0.008$ over the whole range of G_t, it becomes negative for $K_1 = 0.005$ if $G_t \leqslant 0.018$, but it is positive over the whole range of G_t for $K_1 \leqslant 0.002$. However, $R_{20}^{(8)}$ for $\gamma = 30°$ is negative for $K_1 \geqslant 0.010$ over the whole range of G_t, it becomes negative for $K_1 = 0.008$ if $G_t \leqslant 0.038$ and for $K_1 = 0.005$ if $G_t \leqslant 0.016$, but it is positive over the whole range of G_t for $K_1 \leqslant 0.003$. Thus, for certain values of K_1 and G_t, the values of either $R_{20}^{(11)}$ or $R_{20}^{(8)}$ can be very small and positive.

Figure 9 presents the transition boundary between subcritical and supercritical regimes for solutions 11 and 8 for two different values of γ in the (G_t, K_1)-plane. Here $K_2 = 0$ and $G = 1.25$. Each of these solutions is supercritical in the region below its transition curve and subcritical in the region above its transition curve. Thus, just below a transition curve for given K_1 and G_t, the corresponding solution can have very small positive R_{20} and may be preferred over the other solutions.

Supercritical solutions with $R_{10} = 0$

Our present study for the values of K_1 and G_t in the range $0 \leqslant K_1 \leqslant 0.01$ and $0.006 \leqslant G_t \leqslant 0.048$ has detected many supercritical solutions with $R_{10} = 0$ that can compete with one another in the sense that their corresponding R_{20} values can be
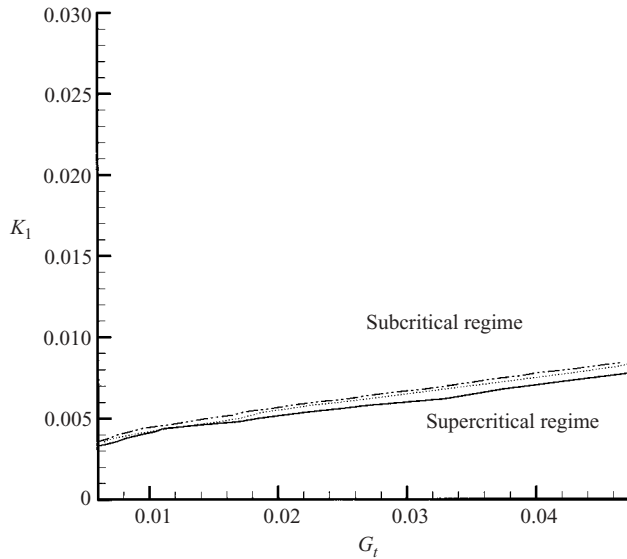
FIGURE 9. Transition boundary between subcritical and supercritical regimes for standing rectangles–steady rectangles in the (G_t, K_1)-plane with $G = 1.25$ and $K_2 = 0$. Here the solid line, dotted line and dash-dot-dot line present the cases of $\gamma = 90°$ (squares), $56°$ and $50°$.

very close to one another for particular values of the parameters. However, it is possible to detect such supercritical solutions with the smallest possible values for their corresponding R_{20} for particular values of the parameters. Table 2 presents the preferred supercritical mixed and simple (non-mixed) solutions, which correspond to the smallest values of R, for $G = 1.25$, $K_2 = 0$ and for different values of G_t and K_1.

We also examined the vertical distribution of solid fraction for a few preferred supercritical mixed solutions, and some typical results are presented for preferred supercritical standing rectangles–steady rectangles for $\gamma = 50°$ in figure 10. This figure presents at $t = 0$ the vertical distribution of the basic state (dotted line), total solid fraction at a down-flow centre (dashed line with a minus sign) and at an up-flow centre (dashed line with a plus sign) and total solid fraction at a down-flow vertex (solid line with a minus sign) and at an up-flow vertex. The parameter values for these results are $\delta = 0.2$, $|\varepsilon| = 0.001$, $G = 1.25$, $G_t = 0.044$, $K_1 = 0.008$ and $K_2 = 0$. It is seen from this figure that the tendency for chimney formation at the vertex is greater in the mid to upper portion of the layer for the down-flow vertex than for the up-flow vertex. However, the tendency for chimney formation exists throughout the layer at an up-flow centre, while no such tendency exists anywhere in the layer at a down-flow centre. Since the sign of the motion at the centres of rectangular cells, or, in general, at the centres of the cells for any supercritical solution with $R_{10} = 0$, alternates from one cell to an adjacent cell (Busse 1967), these results imply that the tendency for chimney formation in a such supercritical flow can be at the vertices as well as at the centres.

4.3. *Stability of finite-amplitude mixed solutions*

Following standard stability procedures (Schluter, Lortz & Busse 1965; Busse 1967), the system of equations for the growth rate σ^* of the mixed and simple disturbances acting on the finite-amplitude mixed or simple solutions have been simplified, and the expression for σ^* has been computed for different integers N and various values of ψ_{nm} ($|\psi_{nm}| \leqslant 1$). In all the cases that have been investigated only supercritical mixed

G_t \\ K_1	0.000	0.001	0.002	0.003	0.004	0.005	0.006	0.007	0.008	0.009	0.010
0.006	sr	6(.3)	sr	9_c(.2)	9c(.4)	sr	sr	sr	sr	sr	sr
0.008	sr	6(.3)	sr	12(.1)	9_b(.3)	9_a(.4)	sr	sr	sr	sr	sr
0.010	sr	sr	sr	sr	9_d(.2)	9_a(.3)	9_b(.4)	sr	sr	sr	sr
0.012	sr	6(.3)	sr	12(.1)	9_c(.3)	9_b(.4)	sr	sr	sr	sr	sr
0.014	sr	6(.3)	sr	12(.1)	9_b(.3)	9_b(.4)	sr	sr	sr	sr	sr
0.016	sr	sr	sr	12(.1)	9_a(.1)	9_c(.4)	sr	sr	sr	sr	sr
0.018	sr	sr	5	sr	12(.1)	9_c(.3)	9_c(.4)	sr	sr	sr	sr
0.020	sr	sr	5	sr	12(.1)	9_a(.1)	8_b	9_a(.4)	sr	sr	sr
0.022	sr	sr	5	sr	12(.1)	9_c(.2)	12(.4)	9_b(.4)	sr	sr	sr
0.024	sr	sr	5	sr	12(.1)	9_b(.2)	8_a	sr	sr	sr	sr
0.026	sr	sr	5	sr	12(.1)	9_c(.1)	9_b(.3)	9_b(.4)	sr	sr	sr
0.028	sr	sr	6(.4)	sr	sr	9_d(.1)	9_c(.3)	8_b	9_a(.4)	sr	sr
0.030	sr	sr	6(.4)	sr	sr	12(.1)	9_a(.1)	9_d(.4)	9_b(.4)	sr	sr
0.032	sr	sr	6(.4)	sr	sr	12(.1)	9_a(.1)	9_d(.4)	9_b(.4)	sr	sr
0.034	sr	sr	6(.4)	sr	sr	12(.1)	9_d(.3)	12(.4)	9_b(.4)	sr	sr
0.036	sr	sr	6(.2)	sr	sr	12(.1)	9_d(.2)	9_c(.3)	9_d(.4)	9_b(.4)	sr
0.038	sr	sr	6(.3)	sr	sr	12(.1)	12(.3)	9_b(.3)	8_a	9_a(.4)	sr
0.040	sr	sr	6(.2)	sr	sr	sr	12(.2)	9_b(.2)	12(.4)	9_b(.4)	9_a(.4)
0.042	sr	sr	6(.2)	sr	sr	sr	9_d(.1)	9_b(.2)	12(.4)	9_b(.4)	9_a(.4)
0.044	sr	sr	6(.3)	5	sr	sr	12(.1)	9_c(.2)	9_b(.3)	9_c(.4)	9_b(.4)
0.046	sr	sr	6(.3)	5	sr	sr	12(.1)	9_c(.2)	9_b(.3)	9_c(.4)	9_b(.4)
0.048	sr	sr	6(.3)	5	sr	sr	12(.1)	9_c(.1)	9_c(.3)	12(.4)	9_b(.4)

TABLE 2. Preferred supercritical solutions for $G = 1.25$, $K_2 = 0$ and different values of G_t and K_1. Here the simple (non-mixed) steady solution in the form of rolls is designated by sr, and the value of the parameter b for the general travelling component of a preferred mixed solution is given in the parentheses. The subscripts a, b, c and d represent, respectively, the angles $\gamma = 15°$, $30°$, $50°$ and $70°$.
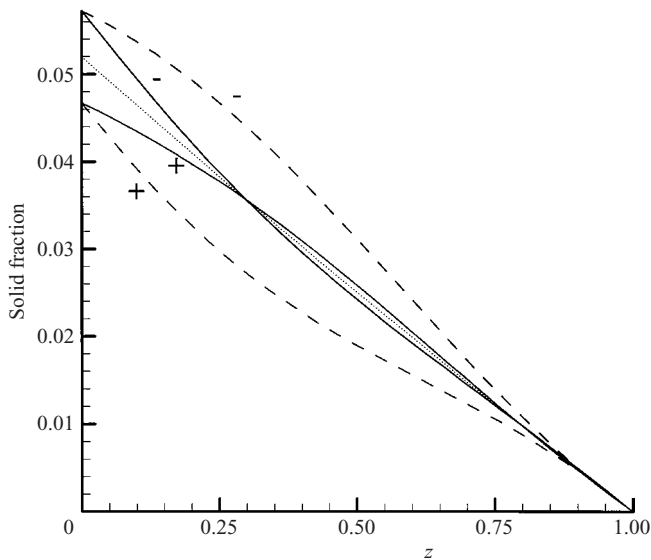

FIGURE 10. Solid fraction versus z for the solution in the form of standing rectangles–steady rectangles with $\gamma = 50°$, $G = 1.25$, $G_t = 0.044$, $K_1 = 0.008$ and $K_2 = 0$. Here dotted line, dashed line ($\pm$) and solid line ($\pm$) present the basic solid fraction ϕ_B, $\tilde{\phi}$ ($x = y = t = 0$, $\varepsilon = \pm 0.001$) and $\tilde{\phi}$ ($x = 1.103$, $y = 2.366$, $t = 1.0$, $\varepsilon = \pm 0.001$), respectively.
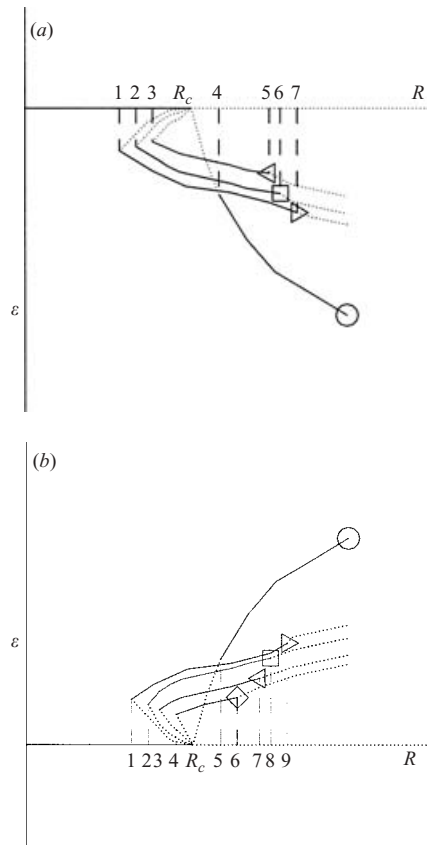
FIGURE 11. Bifurcation diagrams in the (R, ε)-plane. Here the solid line and dotted line present stable and unstable branches, respectively. (*a*) The lines labelled by the symbols represent as follows: ▷ standing down-hexagons–steady down-hexagons; □, general travelling down-hexagons–steady down-hexagons; ◁, simple travelling down-hexagons–steady down-hexagons; and ○, non-hexagonal. (*b*) The lines labelled by the symbols represent as follows: ▷, standing up-hexagons–steady up-hexagons; □, general travelling up-hexagons–steady up-hexagons; ◁, simple travelling up-hexagons–steady up-hexagons; ◇, steady up-hexagons; and ○, non-hexagonal cases.

solutions in the form of mixed rolls, mixed rectangles, mixed squares and simple steady rolls, and subcritical solutions in the form of steady up-hexagons, mixed down-hexagons and mixed up-hexagons are found to be possibly stable in particular range of values of the amplitude of convection and the non-dimensional parameters.

For $K_1 = 0$, no subcritical solution with $R_{10} \neq 0$ is found to be possible and the only stable and preferred solution is that of steady rolls. For $K_1 \neq 0$, the results are briefly as follows. For R above some smallest possible subcritical value ($R < R_c$) for which convection is possible, and below some largest supercritical value ($R > R_c$), the preferred and stable solution is found to be that of subcritical standing hexagons–steady hexagons (solution 2) with down-flow at the cell centres and up-flow at the cell boundaries. Within the stability domain in R for this solution, the solutions are also found to be stable in the following nested-type sequence in the sense that the stability domain of each solution is a sub-domain of that for the previous one: solution 2 with up-flow at the cell centres and down-flow at the cell boundaries, general travelling down-hexagons–steady down-hexagons in the order of increasing $|b|$-values, general

travelling up-hexagons–steady up-hexagons in the order of increasing $|b|$-values, simple travelling down-hexagons–steady down-hexagons followed by simple travelling up-hexagons–steady up-hexagons and steady up-hexagons. It should also be noted that any mixed solution with a general travelling wave component belongs to a class of solutions for different values of b in the range $0 < |b| < 0.5$, and so here we find that many possible solutions can be stable. However, for R just above its smallest possible value where convection is possible, only the standing down-hexagons–steady down-hexagons are realizable and stable and, in practice, are expected to remain the only stable solution in this range of values for R since other possible stable subcritical solutions discussed above may not be realized, unless they are excited due to some initial conditions.

For R above some smallest possible value above R_c, there is close competition between the corresponding supercritical solutions 4–12 with $R_{10} = 0$ which, depending on the particular values for K_1, K_2 and G_t, can become stable, and any stable supercritical solution has the property that its R_{20} coefficient is positive and has the smallest value among all the other supercritical solutions discussed in the previous section. Table 2 provides a list of the preferred and stable supercritical solutions.

Figures 11(*a*) and 11(*b*) provide qualitative bifurcation diagrams for $K_1 \neq 0$ representing the amplitude ε versus R for $\varepsilon < 0$ and $\varepsilon > 0$, respectively, for those solutions which can be preferred and stable in a particular range of R. Solid lines correspond to linearly stable branches, while dotted lines correspond to linearly unstable branches. The numbers 1–3 and 5–7 in figure 11(*a*) designate the boundary values for the range of R in the cases of the stable subcritical solutions with down-flow at the cell centres, while number 4 designates the lower boundary value for R in the case of the supercritical solution. Likewise, the numbers 1–4 and 6–9 in figure 11(*b*) designate the boundary values for the range of R in the cases of the stable subcritical solutions with up-flow at the cell centres, while number 5 designates the lower boundary value for R in the case of the supercritical solution. Note that those solutions that are always unstable are not shown in figure 11. It can be seen from these diagrams that for any supercritical solution, which may become stable for a particular range of the parameter values, one of its branches bifurcates supercritically and is initially unstable to a subcritically bifurcating hexagonal branch.

5. Conclusion and remarks

We have investigated the problem of nonlinear convection due to combined oscillatory and stationary modes, which are referred to as mixed modes, in horizontal mushy layers during the solidification of binary alloys. We considered a particular range of the parameter values where the critical values of the scaled Rayleigh number R for the onset of oscillatory and stationary convection are sufficiently close, and we developed and analysed a nonlinear theory for the mixed modes of convection, which can be either subcritical or supercritical. Twelve new classes of nonlinear mixed solutions are found and their stability investigated. Three of these classes of solutions are subcritical and the other nine are supercritical. For each class of solutions, the oscillatory components of the mixed modes, which could be either a standing wave ($b = 0$), a simple travelling wave ($|b| = 0.5$), or a general travelling wave ($0 < |b| < 0.5$), depend on the parameter b in the range $|b| \leqslant 0.5$. Thus, within each class, there are infinitely many mixed solutions each of which corresponds to a particular value of b in the appropriate domain. The main results for a particular range of relevant parameter values are provided for the preferred solutions, which are stable.

For sufficiently small R or ε, the preferred solution is found to be subcritical and composed of a steady down-hexagonal mode and a standing down-hexagonal mode. It was found that in contrast to the simple type of either oscillatory solutions, where subcritical hexagonal patterns cannot be possible (part 1), or stationary solutions, where down-hexagons cannot be preferred (Amberg & Homsy 1993), the preferred subcritical mixed hexagons with down-flow at the cell centres and up-flow at the cell boundaries are possible and can be stable and realizable over a relatively wide domain in the parameter space.

In regard to the relation of the present mixed-mode problem to simple-mode problems (Amberg & Homsy 1993; Anderson & Worster 1995; part 1), the range of applicability and restrictions in each of these studies should be noted. Amberg & Homsy (1993) restricted their analysis to the case where the non-scaled original Stefan number S_t is an order-one quantity and assumed that δ is of the same order as ε, and they computed stationary solutions in the form of hexagons and rolls only. Their hexagonal solution was determined only to order ε where R_{10} was non-zero for $K_1 \neq 0$. However, R_{10} was zero for rolls, and so they carried out their analysis to order ε^2 to determine the solution for rolls. Their results indicated that $R_{10} < 0$ for steady hexagons, so that steady up-hexagons were subcritical, while steady down-hexagons were supercritical. Hence, the steady solution, which can be preferred and correspond to the smallest value of R, was found to be that of up-hexagons. Anderson & Worster (1995) studied the case where the scaled Stefan number S is an order-one quantity and assumed scalings (2), and they also computed stationary solutions in the form hexagons and rolls only. Similar to the results obtained by Amberg & Homsy (1993), they found that $R_{10} < 0$ for steady hexagons and $R_{10} = 0$ for steady rolls. Hence, again the steady solution, which can correspond to the smallest value of R, is that of up-hexagons if the strict ordering condition $\varepsilon R_{10} \gg \varepsilon \delta R_{11}$ is assumed. However, to explore the possibility for the preference of down-hexagons, which could have some relevance to the experimental observation (Tait *et al.* 1992), Anderson & Worster (1995) found that for K_1 of order δ to the leading term, a range in the parameter values outside that for the available experimental results (Tait *et al.* 1992) existed, where the steady down-hexagons can correspond to the smallest value of R, provided the combined effect of $R_{10} + \delta R_{11}$ is taken into account. In part 1a nonlinear investigation of the simple oscillatory solutions in the particular range of the parameter values where the oscillatory convection can be preferred over the stationary convection was carried out. It was found that $R_{10} = 0$, so that no subcritical solution to order ε was possible. The problem to order ε^2 was then studied and all the solutions to this order were found to be supercritical. The preferred oscillatory solutions, which can correspond to the smallest value of R, were found to be simple travelling rolls ($b = |0.5|$) for most of the relevant range in G_t and standing rolls ($b = 0$) for a very small intermediate range of values for G_t.

The results of the present study for the mixed solutions indicate that the solutions in the form of combined steady down-hexagons and standing down-hexagons can be stable and preferred over a relatively large domain in the parameter space for sufficiently small values of R, which, in particular, covers the values of S and C of the available experimental results due to Tait *et al.* (1992), which are the only available ones known to the author for the planform of weak convection and chimney formation in a mushy layer. Tait *et al.* solidified an ammonium chloride solution in a square tank by slow cooling. For their melt solution and experiment $\delta \approx 1$, $S \approx 5.0$ and $C \approx 20$, which implies $G \approx 1.25$ and $G_t \approx 0.008$. They were able to observe the flow structure near the onset of motion and found that the flow pattern was roughly that

of hexagons with down-flow at the cell centres and up-flow mainly at the nodes of the cells. These flow features were in contrast to the theoretical results by Amberg & Homsy (1993), where the preferred hexagonal cells were found to have up-flow at the cell centres and down-flow at the cell boundaries, and by Anderson & Worster (1995), where a preference for up-hexagons was predicted in a domain where down-hexagons were observed. In part 1 theoretical studies of weakly nonlinear convection in mushy layers were carried out for a particular range of the parameter values where oscillatory modes were demonstrated to be the most critical ones. They showed that no preferred hexagonal convection was possible.

As was demonstrated in part 1, for the parameter regime where the experimental observations are available, both stationary and oscillatory modes need to be taken into account to determine the preferred flow features. Hence, we undertook the present study to arrive at a reasonably complete theory for weak convection in mushy layers. An important result of the present study is the stability of and preference for a mixed solution in the form of standing hexagons–steady hexagons with down flow at the cell centres and up-flow at the cell boundaries in a relatively wide range of the parameter regime, including that of the experiment already carried out. In addition, we found that in contrast to the standing hexagons–steady hexagons with up-flow at the cell centres and down flow at the cell boundaries, our preferred solution in the form of standing down-hexagons–steady down-hexagons exhibits the experimentally observed features of the tendency for chimney formation at the cell nodes at least in the upper portion of the mushy layer. Despite the interesting agreements of the present results with those of the available experimental observation, there are still some restrictions of the present theory due to the modelling assumptions (Amberg & Homsy 1993) and due to the restricted values of R and some other parameters enforced by the present perturbation theory, which may have led to some results whose validity in future experimental observations or in the application to higher values of R cannot be assessed at present. It is hoped that future numerical studies of the fully two-layer system (Worster 1992) for a much wider range of values of R could be carried out to complement and extend the present theory, which could lead to further understanding of the flow features in mushy layers of importance in practical applications and stimulate the future experimental studies.

Appendix

The system of equations and boundary conditions at order ε are as follows:

$$\Delta_2(-\nabla^2 V_{10} + R_{00}\theta_{10} + R_{10}\theta_{00})$$
$$= K_1\left\{\nabla^2(\phi_{00}\Delta_2 V_{00}) + \left(\frac{\partial}{\partial z}\right)\left[\frac{\partial^2 V_{00}}{\partial x\partial z}\frac{\partial\phi_{00}}{\partial x} + \frac{\partial^2 V_{00}}{\partial y\partial z}\frac{\partial\phi_{00}}{\partial y} + \pi^2 V_{00}\frac{\partial\phi_{00}}{\partial z}\right]\right\}, \quad (A\,1a)$$

$$\nabla^2\theta_{10} + G(R_{00}\Delta_2 V_{10} + R_{10}\Delta_2 V_{00} + R_{00}\boldsymbol{\Omega} V_{00}\cdot\nabla\theta_{00}) = 0, \quad (A\,1b)$$

$$S\left[\frac{\partial}{\partial t_1} - \frac{\partial}{\partial z}\right]\phi_{10} + \nabla^2\theta_{10} + R_{00}\Delta_2 V_{10} = -R_{10}\Delta_2 V_{00} - \frac{S\omega_{11}}{\omega_{01}}\frac{\partial\phi_{00}}{\partial t_1} + R_{00}\boldsymbol{\Omega} V_{00}\cdot\nabla\theta_{00},$$
$$(A\,1c)$$

$$V_{10} = \theta_{10} = 0 \quad \text{at} \quad z = 0, \quad (A\,1d)$$

$$V_{10} = \theta_{10} = \phi_{10} = 0 \quad \text{at} \quad z = 1, \quad (A\,1e)$$

where $t_1 = \omega t/\omega_{01}$.

The solvability conditions for system (A1) are reduced to the following two sets of equations:

$$R_{10}(|A_n^+|^2 + |A_n^-|^2)$$

$$= B\frac{2K_1\pi^4}{CG(\sqrt{G})(\pi^2 - \omega_{01}^2)}\sum_{l,p=-N}^{N}(1+\psi_{lp})\{H_p[A_n^+ A_l A_p^+\langle\eta_l\,\eta_p^+\,\eta_n^+\rangle$$

$$+ A_n^- A_l A_p^+\langle\eta_l\,\eta_p^+\,\eta_n^-\rangle] + H_p^*[A_n^+ A_l A_p^-\langle\eta_l\,\eta_p^-\,\eta_n^+\rangle + A_n^- A_l A_p^-\langle\eta_l\,\eta_p^-\,\eta_n^-\rangle]\}$$

$$- B\frac{3K_1\pi^2}{CG\sqrt{G}}\sum_{l,p=-N}^{N}(1+\psi_{lp})\{A_n^+ A_p^+ A_l\langle\eta_p^+\,\eta_l\,\eta_n^+\rangle + A_n^- A_p^+ A_l\langle\eta_p^+\,\eta_l\,\eta_n^-\rangle$$

$$+ A_n^+ A_p^- A_l\langle\eta_p^-\,\eta_l\,\eta_n^+\rangle + A_n^- A_p^- A_l\langle\eta_p^-\,\eta_l\,\eta_n^-\rangle\}, \quad (n=-N,\ldots,-1,1,\ldots,N), \quad (A\,2a)$$

$$R_{10}|A_n|^2 B = \frac{2K_1\pi^4}{CG(\sqrt{G})(\pi^2 - \omega_{01}^2)}\sum_{l,p=-N}^{N}(1+\psi_{lp})[H_p(A_n A_l^+ A_p^+\langle\eta_n\,\eta_l^+\,\eta_p^+\rangle$$

$$+ A_n A_l^- A_p^+\langle\eta_n\,\eta_l^-\,\eta_p^+\rangle) + H_p^*(A_n A_l^+ A_p^-\langle\eta_n\,\eta_l^+\,\eta_p^-\rangle + A_n A_l^- A_p^-\langle\eta_n\,\eta_l^-\,\eta_p^-\rangle)]$$

$$- B\frac{3K_1\pi^2}{CG\sqrt{G}}\sum_{l,p=-N}^{N}(1+\psi_{lp})A_n A_l A_p\langle\eta_n\,\eta_l\,\eta_p\rangle \quad (n=-N,\ldots,-1,1,\ldots,N), \quad (A\,2b)$$

where angular brackets indicate the average over the layer,

$$H_p = \frac{-10\mathrm{i}S_p\omega_{01}}{(3\pi^2)} + \frac{\mathrm{i}S_p\omega_{01}}{4\pi}[\exp(-\mathrm{i}S_p\omega_{01})]\left\{\frac{4\pi[1-\cos(\omega_{01})]}{4\pi^2 - \omega_{01}^2} - \frac{4\pi\mathrm{i}\sin(\omega_{01}S_p)}{4\pi^2 - \omega_{01}^2}\right\}$$

$$- \frac{3}{2}\frac{[1-\exp(-\mathrm{i}\omega_{01}S_p)]}{\mathrm{i}\omega_{01}S_p} + \frac{3}{4}[\exp(-\mathrm{i}\omega_{01}S_p)]$$

$$\times\left\{\frac{-2\omega_{01}S_p\sin(\omega_{01}S_p)}{4\pi^2 - \omega_{01}^2} - \frac{2\mathrm{i}\omega_{01}S_p[1-\cos(\omega_{01})]}{4\pi^2 - \omega_{01}^2}\right\}, \quad (A\,2c)$$

$$\psi_{lp} = \boldsymbol{a}_l\cdot\boldsymbol{a}_p/\pi^2, \quad (A\,2d)$$

and S_p is defined in (8g).

The expressions for the coefficients $C_i^{(1)}(i=1,2,3)$ introduced in (22) for the simple travelling–steady class of detected mixed solutions are

$$C_1^{(1)} = \frac{D_1 C_0/2 - D_2}{\sqrt{6}}, \quad C_2^{(1)} = \frac{D_1 C_0}{\sqrt{6}}, \quad C_3^{(1)} = \frac{D_2}{\sqrt{6}}, \quad D_1 \equiv \frac{2K_1\pi^4}{CG(\pi^2 - \omega_{01}^2)\sqrt{G}},$$

$$D_2 \equiv \frac{3K_1\pi^2}{CG\sqrt{G}}, \quad C_0 \equiv -(\sin\omega_{01}/\omega_{01})\left[3 + \frac{\omega_{01}}{4\pi^2 - \omega_{01}^2}\right]. \quad (A\,3)$$

The expressions for the coefficients $C_i^{(2)}(i=1,2,3)$ of the standing wave–steady class of the mixed solutions are

$$C_1^{(2)} = \frac{D_1 C_0}{\sqrt{6}} - \frac{2D_2}{\sqrt{6}}, \quad C_2^{(2)} = \frac{2D_1 C_0}{\sqrt{6}}, \quad C_3^{(2)} = -\frac{D_2}{\sqrt{6}}, \quad (A\,4)$$

The expressions for the coefficients $C_i^{(3)}$ $(i=1,2,3)$ introduced in (22) for the general travelling–steady class of detected mixed solutions are

$$C_1^{(3)} = \frac{D_1 C_0 b_1}{2\sqrt{6}} - \frac{D_2 b_1}{\sqrt{6}}, \quad C_2^{(3)} = \frac{D_1 C_0 b_1}{\sqrt{6}}, \quad C_3^{(3)} = -\frac{D_2}{\sqrt{6}}, \quad b_1 \equiv 1 + 2(0.25 - b)^{0.5}.$$

$$(A\,5)$$

The expressions for the solutions V_{10}, θ_{10} and ϕ_{10} are given in a supplement to the online version of the paper, also available from the author or the JFM Editorial Office, Cambridge.

The system of equations and boundary conditions at order ε^2 is

$$\Delta_2(-\nabla^2 V_{20} + R_{00}\theta_{20} + R_{10}\theta_{10} + R_{20}\theta_{00})$$

$$= \frac{\partial}{\partial z}[K_1(\boldsymbol{\Omega}\, V_{00}\cdot\nabla\phi_{10} + \boldsymbol{\Omega}\, V_{10}\cdot\nabla\phi_{00}) + K_2\boldsymbol{\Omega}\, V_{00}\cdot\nabla(\phi_{00}^2)]$$

$$+ \nabla^2[K_1(\phi_{10}\Delta_2 V_{00} + \phi_{00}\Delta_2 V_{10}) + K_2\phi_{00}^2\Delta_2 V_{00}], \tag{A 6a}$$

$$\nabla^2\theta_{20} + G\Delta_2(R_{00}V_{20} + R_{10}V_{10} + R_{20}V_{00})$$

$$= G[R_{00}(\boldsymbol{\Omega}\, V_{00}\cdot\nabla\theta_{10} + \boldsymbol{\Omega}\, V_{10}\cdot\nabla\theta_{00}) + R_{10}\boldsymbol{\Omega}\, V_{00}\cdot\nabla\theta_{00}], \tag{A 6b}$$

$$S\left(\frac{\partial}{\partial t_1} - \frac{\partial}{\partial z}\right)\phi_{20} + \Delta_2(R_{00}V_{20} + R_{10}V_{10} + R_{20}V_{00}) + \nabla^2\theta_{20}$$

$$= -\frac{S\omega_{21}}{\omega_{01}}\frac{\partial}{\partial t_1}\phi_{00} - \frac{S\omega_{11}}{\omega_{01}}\frac{\partial}{\partial t_1}\phi_{10} + R_{00}(\boldsymbol{\Omega}\, V_{00}\cdot\nabla\theta_{10} + \boldsymbol{\Omega}\, V_{10}\cdot\nabla\theta_{00}) + R_{10}\boldsymbol{\Omega}\, V_{00}\cdot\nabla\theta_{00}, \tag{A 6c}$$

$$\theta_{20} = V_{20} = 0 \quad \text{at} \quad z = 0, \quad \theta_{20} = V_{20} = \phi_{20} = 0 \quad \text{at} \quad z = 1. \tag{A 6d}$$

The solvability conditions for the system (A 6) are reduced to the following two sets of equations:

$$R_{20}\sqrt{G}\pi(|A_n^+|^2 + |A_n^-|^2)$$

$$= \sum_{m=-N}^{N}\left\{\left[T_{nm}^{(o1)}|A_n^+|^2|A_m^+|^2 + T_{nm}^{(o2)}A_n^- A_m^- A_{-n}^+ A_{-m}^+\delta(S_n + S_m)\right.\right.$$

$$+ T_{nm}^{(o3)}|A_n^-|^2|A_m^+|^2 + T_{nm}^{(o4)}A_n^+ A_m^- A_{-n}^- A_{-m}^+\delta(S_n - S_m) + T_{nm}^{(o5)}A_n^- A_m^+ A_{-n}^+ A_{-m}^-\delta(S_m - S_n)$$

$$+ T_{nm}^{(o6)}|A_n^+|^2|A_m^-|^2 + T_{nm}^{(o7)}A_n^+ A_m^+ A_{-n}^- A_{-m}^-\delta(S_n + S_m) + T_{nm}^{(o8)}|A_n^-|^2|A_m^-|^2]$$

$$+ B^2[T_{nm}^{(o9)}A_n^+ A_m A_{-n} A_{-m}^+\delta(S_n - S_m) + T_{nm}^{(o10)}A_n^- A_m A_{-n} A_{-m}^+\delta(S_n + S_m)$$

$$+ T_{nm}^{(o11)}A_n^+ A_m A_{-n} A_{-m}^-\delta(S_m + S_n) + T_{nm}^{(o12)}A_n^- A_m A_{-n} A_{-m}^-\delta(S_n - S_m)$$

$$+ T_{nm}^{(o13)}|A_n^+|^2|A_m|^2 + T_{nm}^{(o14)}|A_n^-|^2|A_m|^2 + T_{nm}^{(o15)}A_n^+ A_m^+ A_{-n} A_{-m}\delta(S_n + S_m)$$

$$+ T_{nm}^{(o16)}A_n^- A_m^+ A_{-n} A_{-m}\delta(S_m - S_n) + T_{nm}^{(o17)}A_n^+ A_m^- A_{-n} A_{-m}\delta(S_n - S_m)$$

$$\left.\left. + T_{nm}^{(o18)}A_n^- A_m^- A_{-n} A_{-m}\delta(S_n + S_m)]\right\} + BH_1 S, \quad (n = -N, \ldots, -1, 1, \ldots, N), \tag{A 7a}$$

$$R_{20}\sqrt{G}\pi|A_n|^2 B$$

$$= \sum_{m=-N}^{N}\left\{B[T_{nm}^{(s1)}A_n A_m A_{-n}^+ A_{-m}^+\delta(S_n + S_m) + T_{nm}^{(s2)}A_n A_m A_{-n}^- A_{-m}^+\delta(S_n - S_m)\right.$$

$$+ T_{nm}^{(s3)}A_n A_m A_{-n}^+ A_{-m}^-\delta(S_m - S_n) + T_{nm}^{(s4)}A_n A_m A_{-n}^- A_{-m}^-\delta(S_n + S_m)$$

$$+ T_{nm}^{(s5)}|A_n|^2|A_m^+|^2 + T_{nm}^{(s6)}|A_n|^2|A_m^-|^2 + T_{nm}^{(s7)}A_n A_{-m} A_{-n}^+ A_m^+\delta(S_m - S_n)$$

$$+ T_{nm}^{(s8)}A_n A_{-m} A_{-n}^+ A_m^-\delta(S_n + S_m) + T_{nm}^{(s9)}A_n A_{-m} A_{-n}^- A_m^+\delta(S_m + S_n)$$

$$+ T_{nm}^{(s10)}A_n A_{-m} A_{-m}^- A_m^-\delta(S_n - S_m) + B^3[T_{nm}^{(s11)}|A_n|^2|A_m|^2]\}$$

$$+ (H_2 + B^2 H_3)S, \quad (n = -N, \ldots, -1, 1, \ldots, N), \tag{A 7b}$$

where

$$\delta(a) = 1 \quad \text{for} \quad a = 0 \quad \text{and} \quad 0 \quad \text{for} \quad a \neq 0, \tag{A 7c}$$

$$S = 1 \text{ for hexagons and } 0 \text{ for non-hexagons.} \tag{A 7d}$$

Here the term 'non-hexagons' in (A 7d) means solutions whose wavenumber vectors do not contain a sub-set of such vectors, which can satisfy a condition of the type (20a). The expressions for the coefficients $T_{nm}^{(oi)}$ ($i = 1, \ldots, 18$), $T_{nm}^{(sj)}$ ($j = 1, \ldots, 11$) and H_k ($k = 1, 2, 3$) are too lengthy and will not be given in this paper.

The stability system is

$$\nabla^2 \left[\varepsilon \phi' \left(\frac{\mathrm{d}}{\mathrm{d}\tilde{\phi}} \right) K(\tilde{\phi}) \Delta_2 V + K(\tilde{\phi}) \Delta_2 V' \right]$$

$$+ \frac{\partial}{\partial z} \left\{ \varepsilon \boldsymbol{\Omega} V \cdot \nabla \left[\phi' \left(\frac{\mathrm{d}}{\mathrm{d}\tilde{\phi}} \right) K(\tilde{\phi}) \right] + \boldsymbol{\Omega} V' \cdot \nabla K(\tilde{\phi}) \right\} - R \Delta_2 \theta' = 0, \tag{A 8a}$$

$$\left(\frac{\partial}{\partial t} + \sigma - \frac{\delta \partial}{\partial z} \right) \left(-\theta' + \frac{S\phi'}{\delta} \right) + R \left(\frac{\mathrm{d}\theta_B}{\mathrm{d}z} \right) \Delta_2 V' + \nabla^2 \theta' = \varepsilon R (\boldsymbol{\Omega} V \cdot \nabla \theta' + \boldsymbol{\Omega} V' \cdot \nabla \theta), \tag{A 8b}$$

$$\left(\frac{\partial}{\partial t} + \sigma - \delta \frac{\partial}{\partial z} \right) \left[(-1 + \phi_B)\theta' + \theta_B \phi' + \varepsilon \phi \theta' + \varepsilon \phi' \theta - \frac{C\phi'}{\delta} \right] + R \left(\frac{\mathrm{d}\theta_B}{\mathrm{d}z} \right) \Delta_2 V'$$

$$= \varepsilon R (\boldsymbol{\Omega} V \cdot \nabla \theta' + \boldsymbol{\Omega} V' \cdot \nabla \theta), \tag{A 8c}$$

$$V' = \theta' = 0 \quad \text{at} \quad z = 0, \tag{A 8d}$$

$$V' = \theta' = \phi' = 0 \quad \text{at} \quad z = 1. \tag{A 8e}$$

REFERENCES

AMBERG, G. & HOMSY, G. M. 1993 Nonlinear analysis of buoyant convection in binary solidification with application to channel formation. *J. Fluid Mech.* **252**, 79–98.

ANDERSON, D. M. & WORSTER, M. G. 1995 Weakly nonlinear analysis of convection in mushy layers during the solidification of binary alloys. *J. Fluid Mech.* **302**, 307–331.

ANDERSON, D. M. & WORSTER, M. G. 1996 A new oscillatory instability in a mushy layer during the solidification of binary alloys. *J. Fluid Mech.* **307**, 245–267.

BUSSE, F. H. 1967 The stability of finite amplitude convection and its relation to an extremum principal. *J. Fluid Mech.* **30**, 625–649.

BUSSE, F. H. 1975 Patterns of convection in spherical shells. *J. Fluid Mech.* **72**, 67–85.

BUSSE, F. H. 1989 Fundamentals of thermal convection. In *Mantle Convection, Plate Tectonics and Global Dynamics* (ed. W. R. Peltier), pp. 23–95. Gordon and Breach.

BUSSE, F. H. & RIAHI, D. N. 1988 Mixed-mode patterns of bifurcations from spherically symmetric basic states. *Nonlinearity* **1**, 379–388.

CHANDRASEKHAR, S. 1961 *Hydrodynamic and Hydromagnetic Stability.* Clarendon.

RIAHI, D. N. 1983 Nonlinear convection in a porous layer with finite conducting boundaries. *J. Fluid Mech.* **129**, 153–171.

RIAHI, D. N. 2002 On nonlinear convection in mushy layers. Part 1. Oscillatory modes of convection. *J. Fluid Mech.* **467**, 331–359.

SCHLUTER, A., LORTZ, D. & BUSSE, F. H. 1965 On the stability of finite amplitude convection. *J. Fluid Mech.* **23**, 129–144.

TAIT, S., JAHRLING, K. & JAUPART, C. 1992 The planform of compositional convection and chimney formation in a mushy layer. *Nature* **359**, 406–408.

WORSTER, M. G. 1992 Instabilities of the liquid and mushy regions during solidification of alloys. *J. Fluid Mech.* **237**, 649–669.